# DEEP SPITZER $24\,\mu m$ COSMOS IMAGING – I. THE EVOLUTION OF LUMINOUS DUSTY GALAXIES - CONFRONTING THE MODELS

Emeric Le Floc'h[1,2], Hervé Aussel[3], Olivier Ilbert[1,4], Laurie Riguccini[1,3], David T. Frayer[5], Mara Salvato[6], Jason Surace[7], Stephane Arnouts[8], Chiara Feruglio[3], Giulia Rodighiero[9], Peter Capak[6,7], Jeyhan Kartaltepe[1], Sebastien Heinis[10], Kartik Sheth[7], Lin Yan[7], Henry Joy McCracken[11], David Thompson[12], David Sanders[1], Nick Scoville[6], Anton Koekemoer[13]

*Accepted to The Astrophysical Journal, 22 July 2009*

## ABSTRACT

We present the first results obtained from the identification of $\sim 30\,000$ sources in the *Spitzer*/$24\,\mu m$ observations of the COSMOS field at $S_{24\mu m} \gtrsim 80\,\mu$Jy. Using accurate photometric redshifts ($\sigma_z \sim 0.12$ at $z \sim 2$ for $24\,\mu m$ sources with $i^+ \lesssim 25\,$mag AB) and simple extrapolations of the number counts at faint fluxes we resolve with unprecedented detail the build-up of the mid-infrared background across cosmic ages. We find that $\sim 50\%$ and $\sim 80\%$ of the $24\,\mu m$ background intensity originate from galaxies at $z \lesssim 1$ and $z \lesssim 2$ respectively, supporting the scenario where highly obscured sources at very high redshifts ($z \gtrsim 2$) contribute only marginally to the Cosmic Infrared Background. Assuming flux-limited selections at optical wavelengths, we also find that the fraction of $i^+$–band sources with $24\,\mu m$ detection strongly increases up to $z \sim 2$ as a consequence of the rapid evolution that star-forming galaxies have undergone with lookback time. Nonetheless this rising trend shows a clear break at $z \sim 1.3$, probably due to $k$-correction effects implied by the complexity of spectral energy distributions in the mid-infrared. Finally, we compare our results with the predictions from different models of galaxy formation. We note that semi-analytical formalisms currently fail to reproduce the redshift distributions observed at $24\,\mu m$. Furthermore the simulated galaxies at $S_{24\mu m} > 80\,\mu$Jy exhibit $R - K$ colors much bluer than observed and the predicted $K$–band fluxes are systematically underestimated at $z \gtrsim 0.5$. Unless these discrepancies mainly result from an incorrect treatment of extinction in the models they may reflect an underestimate of the predicted density of high redshift massive sources with strong on-going star formation, which would point to more fundamental processes and/or parameters (e.g., Initial Mass Function, critical density to form stars, feedback, ...) that are still not fully controlled in the simulations. The most recent backward evolution scenarios reproduce reasonably well the flux/redshift distribution of $24\,\mu m$ sources up to $z \sim 3$, although none of them is able to exactly match our results at all redshifts.

*Subject headings:* galaxies: high-redshift — infrared: galaxies — cosmology: observations

## 1. INTRODUCTION

Over the last decade, extragalactic infrared (IR) surveys have become a key component in our quest to un-

[1] Institute for Astronomy, University of Hawaii, 2680 Woodlawn Drive, Honolulu, HI 96822, USA
[2] Spitzer fellow
[3] UMR AIM (CEA–UP7–CNRS), CEA-Saclay, Orme des Merisiers, bât. 709, F-91191 Gif-sur-Yvette Cedex, France
[4] Laboratoire d'Astrophysique de Marseille, BP 8, Traverse du Siphon, 13376 Marseille Cedex 12, France
[5] Infrared Processing and Analysis Center, California Institute of Technology 100-22, Pasadena, CA 91125, USA
[6] California Institute of Technology, MC 105-24, 1200, East California Boulevard, Pasadena, CA 91125, USA
[7] Spitzer Science Center, California Institute of Technology, Pasadena, CA 91125, USA
[8] Canada France Hawaii telescope corporation, 65-1238 Mamalahoa Hwy, Kamuela, Hawaii 96743, USA
[9] Dipartimento di Astronomia, Università di Padova, Vicolo Osservatorio 2, I-35122, Padova, Italy
[10] Johns Hopkins University, Bloomber Center #380, 3400 N. Charles Street, Baltimore MD 21218, USA
[11] Institut d'Astrophysique de Paris, UMR7095 CNRS, Université Pierre et Marie Curie, 98 bis Boulevard Arago, 75014 Paris, France
[12] LBT Observatory, University of Arizona, 933 N. Cherry Ave., Tucson, Arizona, 85721-0065, USA
[13] Space Telescope Science Institute, 3700 San Martin Drive, Baltimore MD 21218, USA
Electronic address: elefloch@ifa.hawaii.edu

derstand galaxy formation. The reprocessing of stellar and nuclear radiations by dust and the resulting emission of this energy at thermal IR wavelengths ($8\,\mu m \lesssim \lambda \lesssim 1000\,\mu m$) plays a major role in shaping the panchromatic appearance of star-forming galaxies and active galactic nuclei (e.g., Silva et al. 1998; Gordon et al. 2000; Nenkova et al. 2002; Dopita et al. 2005; Marshall et al. 2007; Siebenmorgen & Krügel 2007; da Cunha et al. 2008). The direct characterization of the properties of these sources at IR wavelengths is therefore crucial for reliably estimating the fraction of their bolometric energy output absorbed by dust and converted into lower energy photons. It also provides unique constraints on the nature of the different physical processes driving their on-going activity (e.g, de Grijp et al. 1985; Mazzarella et al. 1991; Genzel et al. 1998; Dale et al. 2006; Smith et al. 2007; Spoon et al. 2007).

The discovery of a large number of distant sources radiating copious amounts of energy in the IR (e.g., Smail et al. 1997; Barger et al. 1998; Aussel et al. 1999; Elbaz et al. 1999; Blain et al. 2002; Papovich et al. 2004; Dole et al. 2004; Daddi et al. 2005) revealed that critical phases of the cosmic star formation and nuclear accretion history happened within dust-embedded environments hidden behind large amounts of absorbing material. A significant fraction of the growth of structures over cos-

mic ages thus occurred in galaxies affected by substantial reddening and which characterization at shorter wavelengths (e.g., UV, optical) can be severely biased if their extinction is not properly estimated. At large cosmological distances, highly obscured sources can even be barely detectable below $\sim 1\,\mu$m and the observations in the IR or the millimeter are sometimes the only way to unveil the presence of on-going star formation and/or nuclear activity in these galaxies (e.g., Hughes et al. 1998; Downes et al. 1999; Houck et al. 2005).

The infrared spectral energy distributions (SED) of star-forming galaxies and active galactic nuclei (AGN) usually peak at $\sim 80$–$200\,\mu$m. The most reliable estimate of the energy absorbed by dust in these sources would thus require observations in the far-IR or the submillimeter. Unfortunately though, data taken at such wavelengths have been so far hampered by source confusion as well as the very modest sensitivity of current detectors and the difficulty to access this frequency range from the ground. For instance, observations of the distant Universe performed at $70\,\mu$m and $160\,\mu$m with the *Spitzer Space Telescope* (Werner et al. 2004) or in the submillimeter with ground-based cameras of bolometers have been so far limited to the identification of galaxies at the very bright end of the luminosity function (i.e., $L_{bol} \gtrsim 10^{12}\,L_\odot$), with biases due to dust temperature selection effects (e.g., Blain et al. 2004; Frayer et al. 2006; Pope et al. 2006; Borys et al. 2006; Le Floc'h et al. 2007). Detecting the more typical high redshift sources at the peak of their IR SED has not been achieved yet, and our knowledge of the far-IR luminosity function of galaxies in the distant Universe is still affected by substantial uncertainties.

This strong limitation can be partially remedied with observations performed at mid-IR wavelengths (i.e., $5\,\mu$m $\lesssim \lambda \lesssim 60\,\mu$m). Although cameras operating in the mid-IR are not as efficient as optical detectors they have been far more sensitive than in the far-IR, allowing the probe of the IR luminosity function down to much fainter levels. The observed correlations between the mid-IR and the far-IR luminosities of star-forming galaxies allow reasonable estimates of their total IR luminosity ($L_{IR} = L_{8-1000\mu m}$) with extrapolations from fluxes measured in the mid-IR (Spinoglio et al. 1995; Chary & Elbaz 2001; Bavouzet et al. 2008; Symeonidis et al. 2008). At such wavelengths, starbursts and AGNs exhibit also quite disctinct spectral signatures, providing invaluable clues to quantify the relative contribution of star-forming and nuclear activity occurring within individual sources.

Observations of the deep Universe with the $24\,\mu$m bandpass of the *Multi-band Imaging and Photometer for Spitzer* (MIPS, Rieke et al. 2004) and with the *Infrared Spectrograph* (IRS, Houck et al. 2004) have led to tremendous progress in our understanding of the bolometric properties of distant sources (e.g., Huang et al. 2005; Yan et al. 2005; Daddi et al. 2005; Papovich et al. 2006; Webb et al. 2006; Reddy et al. 2006; Menéndez-Delmestre et al. 2007; Sajina et al. 2007; Lutz et al. 2008; Pope et al. 2008). The *Spitzer* data provide tight constraints on the different mechanisms (merging, feedback, environmental effects) that regulate the activity of star formation and nuclear accretion in galaxies (e.g., Noeske et al. 2007; Elbaz et al. 2007; Bridge et al. 2007; Buat et al. 2008; Bai

et al. 2007; Marcillac et al. 2008). They also enable the identification of a large number of obscured AGNs that must have played a key role in driving the coeval growth of bulges and super-massive black holes but whose contribution is usually underestimated by surveys performed at other wavelengths (e.g., Houck et al. 2005; Polletta et al. 2006; Alonso-Herrero et al. 2006; Dey et al. 2008; Fiore et al. 2008).

In spite of this wealth of results recently achieved with *Spitzer* at mid-IR wavelengths, a coherent and comprehensive picture of the deep IR Universe is still missing though. Given the variety of starburst and AGN SEDs in the mid-IR (e.g., Laurent et al. 2000; Brandl et al. 2006; Weedman et al. 2005; Wu et al. 2006; Armus et al. 2007), observations at these wavelengths are affected by quite complex $k$-correction effects and their sensitivity decreases rapidly beyond $z \sim 1$. Hence, wide and shallow surveys are only sensitive to the very bright end of the mid-IR luminosity function, while the deeper observations usually performed at the expense of the covered area suffer from limited statistics. Also, the identification of mid-IR selected sources at high redshift can be extremely difficult given their faintness at optical wavelengths. As a result the exact role that dusty galaxies played with respect to the less luminous but much more numerous sources at the faint end of the luminosity function is still under debate (but see Reddy et al. 2008).

In the attempt to unify the different pictures of galaxy evolution recently achieved by optical and IR surveys we undertook deep $24\,\mu$m imaging over the whole area of the COSMOS field using the MIPS instrument on-board *Spitzer*. The *Cosmic Evolution Survey* (COSMOS) is designed to probe the evolution of galaxies and AGNs up to $z \sim 6$ over a sky region large enough to address the role of environment and large scale structures (Scoville et al. 2007b). It is based on deep multi-wavelength observations performed over $\sim 2\,deg^2$ from the X-ray to radio wavelengths (Hasinger et al. 2007; Taniguchi et al. 2007; Sanders et al. 2007; Bertoldi et al. 2007; Schinnerer et al. 2007), with additional support from high spatial resolution imaging obtained with the *Hubble Space Telescope* (Scoville et al. 2007a; Koekemoer et al. 2007). Intensive spectroscopic follow-up was also carried out with the *Very Large Telescope* (Lilly et al. 2007) while photometric redshifts with unprecedented accuracy were determined for more than $\sim 900\,000$ $i^+$–band selected galaxies in the field (Ilbert et al. 2009). The quality of the data sets available in COSMOS (and in particular the depth with respect to the covered area) is therefore very well suited for probing the multi-wavelength properties of galaxies with minimized cosmic variance and over a wide range of redshifts and luminosities.

In this paper we present our very first analysis of the mid-IR selected galaxy population detected down to $S_{24\mu m} \sim 80\,\mu$Jy in COSMOS. Data are described in Sect. 2 and our $24\,\mu$m source number counts are shown in Sect. 3. Using the photometric redshifts of Ilbert et al. (2009) and Salvato et al. (2009) we then determine the $24\,\mu$m redshift distributions in Sect. 4 and we analyze the number counts as a function of cosmic time in Sect. 5 to constrain the history and the build-up of the Cosmic Infrared Background (CIB). In Sect. 6 we present comparisons between the observed $24\,\mu$m source redshift distributions and the predictions from both phenomeno-

logical and semi-analytical scenarios of galaxy formation. The results are discussed in Sect. 7, which allows us to quantify how well the contribution of dusty luminous sources as a general population is currently understood in models of galaxy evolution. Future papers will be dedicated to the analysis of the multi-wavelength properties of the COSMOS mid-IR selected galaxies, their evolution, their clustering and their connection with sources selected with other criteria. Throughout this paper we assume a $\Lambda$CDM cosmology with $H_0 = 70$ km s$^{-1}$ Mpc$^{-1}$, $\Omega_m = 0.3$ and $\Omega_\lambda = 0.7$ (Spergel et al. 2003). Magnitudes are quoted in AB[14] unless the use of the Vega system is explicitly stated (e.g., Sect. 6.1).

## 2. THE DATA

### 2.1. *The 24 $\mu$m observations of COSMOS*

#### 2.1.1. *Data acquisition and reduction*

The COSMOS field was observed at $24\,\mu$m with the MIPS instrument on-board *Spitzer* as part of two General Observer programs (PI D. Sanders). The first observations (GO2, PID 20070) were carried out in January 2006 with the MIPS medium scan mode and two scan passes per sky pixel. As described in more detail by Sanders et al. (2007) this shallow imaging covered a total area of $\sim 4\,$deg$^2$ centered on COSMOS, with a median integration time of $80\,$s per pixel. This first program was also used to test in a small region of the field the feasibility to improve the $24\,\mu$m sensitivity with longer integrations despite the COSMOS mid-IR background being $\sim 2\times$ higher than in other typical "cosmological" fields (e.g., *Hubble/Chandra Deep Fields*, Lockman Hole). After validating this additional step, deeper imaging was performed in 2007 over the whole COSMOS field as part of a second program using the MIPS slow scan mode (GO3, PID 30143). These data yielded a second and independent $24\,\mu$m coverage over a total area of $\gtrsim 3\,$deg$^2$. Across the nominal $2\,$deg$^2$ of COSMOS the combination of the GO2 and GO3 observations results in a median integration time of $\sim 3\,360\,$s per sky pixel. Note that the MIPS scan mode provides simultaneous imaging at 24, 70 and $160\,\mu$m; the observations of the COSMOS field at $70/160\,\mu$m are presented by Frayer et al. (submitted to AJ).

All the data set was reduced following the procedure outlined in Sanders et al. (2007). For each observing campaign a background pattern derived for every scan mirror position of the instrument was scaled and subtracted from all individual frames. These background-subtracted images were then interpolated to a common grid of pixels using the MOPEX package (Makovoz & Khan 2005). They were finally coadded with our own IDL routines using the median of all the pixels associated with each sky position. We stress that the use of a median combination was necessary in order to reject moving sources present in the field at the time of the observations. A forthcoming paper (Aussel et al. in prep.) will describe in more detail the data reduction. It will also provide a list of the $24\,\mu$m–detected asteroids in COSMOS.

#### 2.1.2. *24 $\mu$m source extraction, photometry*

[14] mag (AB) = $-2.5 \times \log_{10}$ [$F_\nu$ (mJy)] $+16.4$.

The $24\,\mu$m sources in our mosaic were detected using the automatic procedure of the Sextractor software (Bertin & Arnouts 1996) and we measured their flux densities with the Point Spread Function (PSF) fitting technique of the DAOPHOT package (Stetson 1987). Given the Full-Width at Half Maximum (FWHM) of the MIPS-$24\,\mu$m PSF ($\sim 6''$), most of the sources are not resolved in our data. In deep and crowded images such as the ones typically obtained in the MIPS deep surveys, the PSF fitting thus provides more reliable flux measurements than aperture photometry. Furthermore, DAOPHOT performs simultaneous fits to multiple objects, which ensures a proper separation of blended sources especially when the fluxes are close to the confusion limit. No prior information from any other wavelength was used for the source detection itself. However, several PSF fitting iterations were necessary to achieve a clean extraction of the blended sources that were not properly identified by Sextractor in the input $24\,\mu$m image. In brief, these blended cases were located (with Sextractor again) as positive detections in the residual mosaic obtained after the first PSF fitting. Their positions were added to the initial list of $24\,\mu$m sources determined with Sextractor and another extraction of the initial COSMOS $24\,\mu$m image was then performed. Three iterations of this process were carried out, until the residual mosaic was cleaned from any positive signal above the detection threshold chosen for Sextractor. The result of this PSF fitting is illustrated in Figure 1. It shows a sub-region of our COSMOS $24\,\mu$m mosaic along with the corresponding residual image obtained after subtracting all sources extracted with DAOPHOT.

To run this PSF fitting we built an empirical PSF from the brightest point sources identified in the mosaic and we subsequently fit this PSF to every single object detected by Sextractor. DAOPHOT performs this fit by scaling the empirical PSF within a fixed circular aperture centered on the source and it provides the flux of the fitted PSF *enclosed within this aperture*. Therefore a correction must be applied to account for the spatially-extended wings of the PSF lying beyond the radius of the chosen aperture. This correction was determined using the MIPS-$24\,\mu$m STiny Tim PSF models provided by the *Spitzer Science Center*. These models allow to account for the fraction of energy lying at large radii where the signal to noise in our data is not large enough to constrain the exact profile of the Point Spread Function. Relying on such corrections we believe that our flux absolute calibration should be accurate within a few percent, which is consistent with the results obtained by Engelbracht et al. (2007) and Rieke et al. (2008) as part of the calibration of the MIPS $24\,\mu$m detector.

Following the convention adopted by the *Spitzer Science Center* we assumed a stellar $10\,000\,$K black-body spectrum as the reference underlying SED for the $24\,\mu$m flux density measurements. We tested this calibration by cross-correlating our source list with the stars of the *Two Micron All Sky Survey* (2MASS) catalog (Jarrett et al. 2000). Our comparison did not reveal any systematic deviation from the relation $K_s - [24] = 0$ (Vega, with [24] denoting the equivalent magnitude measured in the $24\,\mu$m MIPS bandpass), which is expected for most of the stellar spectral types when no dust emission excess is detected above the photospheric stellar emission

-1.08 μJy/arcsec²                    0.0 μJy/arcsec²                    1.0 μJy/arcsec²                    2.17 μJy/arcsec²
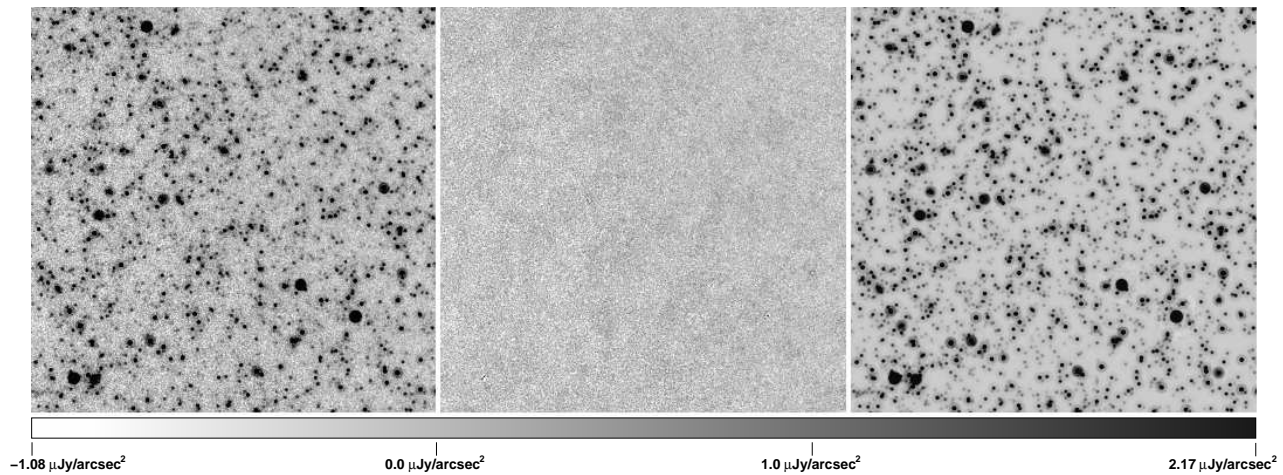
FIG. 1.— A 15'×15' sub-region of the COSMOS field observed at $24\,\mu$m (left panel), along with the residual image obtained on the same field of view after subtracting sources with a PSF fitting technique (central panel). The "reconstructed" image derived with this PSF fitting is shown on the right panel.

(e.g., Gorlova et al. 2006). This cross-correlation also allowed us to register the absolute astrometric calibration of our $24\,\mu$m mosaic to the 2MASS astrometric system. This was performed by applying a systematic offset of $\delta\,\mathrm{Dec} = -0.3''$ to the astrometry derived from the *Spitzer* data products.

The noise in the final $24\,\mu$m mosaic was characterized using two different methods. First, we computed the dispersion of a set of random flux measurements performed over blank field regions of the COSMOS $24\,\mu$m image within the same aperture as the one used for the PSF fitting. Similar to the photometry measurements described above a flux correction was applied to account for the extent of the PSF lying outside of the aperture, which led to an equivalent sensitivity limit of $1\sigma = 18\,\mu$Jy. Second, we also performed a number of simulations adding artificial point-like sources in blank field regions of the mosaic. We measured the fluxes of these sources with the PSF fitting of DAOPHOT and the distribution of the differences between their measured and input fluxes was fitted with a gaussian function. Our best fit was obtained for a $1\sigma$ standard deviation varying between $14\,\mu$Jy and $16\,\mu$Jy depending on the range of input fluxes. Using these simulations we finally examined the robustness of the error measurements provided by our PSF fitting by comparing the DAOPHOT uncertainties obtained for the simulated point sources with the errors directly estimated from the differences between their measured and input fluxes. We applied a systematic scaling of 3.8 to all the DAOPHOT errors so as to get 68% of the distribution of these differences within the DAOPHOT $1\sigma$ uncertainties.

The completeness of our $24\,\mu$m source extraction was determined using the same point source simulations as the ones described in the previous paragraph. We inserted within the mosaic a set of empirical PSFs that were scaled to provide a flux distribution representative of the one characterizing the $24\,\mu$m extragalactic source population. These PSFs were subsequently extracted following the same method as the one employed to detect and to measure the flux of the sources already present in the $24\,\mu$m image. We found that our source extraction is more than 90% complete above a $24\,\mu$m flux

$S_{24\mu m} \sim 80\,\mu$Jy, which should thus be considered as a safe and conservative flux limit for any analysis requiring an unbiased $24\,\mu$m selection of sources in the COSMOS field. According to the simulations though, our PSF fitting is still reliable down to fluxes as faint as $\sim 60\,\mu$Jy and in spite of a lower completeness ($\sim 75\%$) our source extraction should suffer from a relatively small contamination by fake objects at these flux levels.

Based on this characterization we defined our final COSMOS MIPS-$24\,\mu$m catalog as the population of $24\,\mu$m sources brighter than $60\,\mu$Jy lying within the area covered by the COSMOS photometric redshift catalog of Ilbert et al. (2009, see section 2.3) but outside of the masked regions defined from the Subaru optical observations of the COSMOS field. These masked areas cover a surface as large as $0.26\,\mathrm{deg}^2$ but the optical photometry in these regions is affected by larger uncertainties due to the presence of very bright or even saturated objects. In particular, the photometric redshifts in these areas are less accurate. Keeping these regions would thus compromise our analysis of the MIPS-selected galaxies given the large fraction of $24\,\mu$m sources associated with faint optical counterparts. Our $24\,\mu$m catalog represents a total of $39\,413$ sources covering an effective area of $1.68\,\mathrm{deg}^2$. In the remaining of this Section 2 we will describe the identification of the $24\,\mu$m source counterparts down to $S_{24\mu m} = 60\,\mu$Jy. This characterization will supplement other studies carried out by our team using selections performed at other wavelengths. However, the analysis reported in some other sections of this current paper assume an unbiased $24\,\mu$m selection and only sources above $80\,\mu$Jy will be considered in this case.

## 2.2. *Identification of 24 μm source counterparts*

To ensure the most reliable and most complete identification of the $24\,\mu$m source counterparts, we first correlated the $24\,\mu$m data with the $K_s$–band COSMOS catalog of McCracken et al. (submitted to ApJ). As we will see later a non-negligible fraction of the $24\,\mu$m sources at $z \gtrsim 1$ are associated with extremely faint optical counterparts. A direct cross-correlation between the MIPS-$24\,\mu$m and the optical catalogs of COSMOS would thus

result in a lower rate of identifications. Furthermore, the larger uncertainties affecting the determination of source centroids at faint $24\,\mu$m fluxes, the width of the $24\,\mu$m PSF and the very high density of optical sources in our data (e.g., $\sim 45$ galaxies arcmin$^{-2}$ for $i^{+}_{\mathrm{AB}} < 25$ mag in the Subaru COSMOS observations, Taniguchi et al. 2007; Capak et al. 2007) could lead to lots of wrong associations if these identifications had to rely on a direct match between the $24\,\mu$m and optical source catalogs. On the contrary, the COSMOS $K_s$–band catalog is deep enough ($K_s \sim 23.7$ mag at $5\sigma$, McCracken et al.) to detect counterparts for the majority of the $24\,\mu$m selected sources down to our MIPS sensitivity limit. The density of $K_s$–band sources is also substantially smaller ($\sim 7$ galaxies arcmin$^{-2}$ for $K_s < 22$ mag) than in the optical bands and the near-IR wavelengths are "closer" to the $24\,\mu$m bandpass, which minimizes the risk of wrong associations between mid-IR and $K_s$-selected sources. Finally we note that these $K_s$–band observations of COSMOS were executed under excellent seeing conditions ($\sim 0.7''$ at $2.2\,\mu$m). Compared to the other COSMOS near-IR data taken with e.g., the IRAC instrument (FWHM $\sim 1.6''$ at $3.6\,\mu$m, Sanders et al. 2007), the PSF in the $K_s$–band image is much narrower and allows more robust identifications in the case of sources blended at $24\,\mu$m.

We correlated the $24\,\mu$m and $K_s$–band catalogs with a matching radius of $2''$. We found that this distance was large enough to enable the identification of most of the $24\,\mu$m sources, taking into account the width of the $24\,\mu$m PSF (FWHM $\sim 6''$) and the uncertainty on the astrometric position of each single $24\,\mu$m source. This radius was nonetheless sufficiently small to minimize the fraction of multiple matches as well as the association between objects randomly-aligned on the sky. Among the $39\,413$ MIPS–$24\,\mu$m sources of the catalog, we identified a single $K_s$–band counterpart for $33\,146$ objects (84% of the sample) while two possible matches were obtained for $4\,470$ other $24\,\mu$m detections ($\sim 11.5\%$). For theses cases we kept the closest possible counterpart when its centroid was at least twice closer to the $24\,\mu$m source than the second possible match ($2\,320$ objects) while additional priors from the COSMOS IRAC-$3.6\,\mu$m observations were considered to assign the most likely counterpart to the other $24\,\mu$m detections. No association was found for the remaining $1\,797$ sources (4.5% of the catalog). A cross-correlation between these unidentified sources and our $3.6\,\mu$m catalog using the same matching radius revealed IRAC counterparts for 437 objects, a rare population that must be characterized by extremely steep SEDs between $2\,\mu$m and $24\,\mu$m. For the other sources a visual inspection of our data showed that some of them may have counterparts either fainter than the detection thresholds of our $K_s$/IRAC COSMOS catalogs or with a centroid located slightly beyond our $2''$ matching radius. Many of the unidentified objects have also a signal/noise below $5\sigma$ at $24\,\mu$m. At the faintest $24\,\mu$m flux leves some could originate from a small contamination of our catalog by fake sources. It should however not significantly bias our subsequent results given the small fraction that they represent among the whole sample of $24\,\mu$m sources. In summary we identified secure $K_s$–band counterparts for $\sim 90\%$ of the COSMOS $24\,\mu$m catalog down to $60\,\mu$Jy, while less robust identifications were still found for another 5.5% of the MIPS-$24\,\mu$m source population.

Finally we note that this cross-identification with near-IR data also revealed 53 pairs of $24\,\mu$m sources associated with the same $K_s$–band counterpart. A careful inspection of the $24\,\mu$m mosaic revealed that they correspond to single objects incorrectly deblended by the PSF fitting performed in the MIPS data. These "double" components were merged together to form a unique $24\,\mu$m source, reducing the MIPS-selected catalog to $39\,360$ objects.

### 2.3. Photometric redshifts
#### 2.3.1. Input catalogs

The distance of the $24\,\mu$m sources was characterized using the photometric redshifts derived by Ilbert et al. (2009) and Salvato et al. (2009) for the optically and X-ray selected sources of the COSMOS field. These photometric redshifts were determined with deep photometry (e.g., Capak et al. 2009, in preparation) performed in a total of 30 large, medium and narrow band filters over a wavelength range covering the far-UV at 1550Å up to the mid-IR at $8.0\,\mu$m. This large amount of data and the high quality of the observations used in their work resulted in a substantial improvement of photometric redshift accuracy with respect to the determination of redshifts performed in other fields.

The catalog of Ilbert et al. (2009, hereafter I09) provides redshifts for $933\,789$ sources selected at $i^{+}_{\mathrm{AB}} < 26.5$ mag from the Subaru/Suprime–CAM observations of COSMOS, with a dispersion as small as $\sigma_{\Delta z/(1+z)} = 0.012$ for $i^{+}_{\mathrm{AB}} < 24$ mag and $z < 1.25$. This unprecedented accuracy in photometric redshift determinations was mostly achieved thanks to the high sampling of the observed spectral energy distribution of sources around the position of their Balmer break as well as a new method accounting for the contribution of emission lines to their measured flux densities. As shown by Ilbert et al. (2009) the uncertainties affecting their redshift estimates depend primarily on the redshift and the apparent $i^{+}$–band magnitude of sources (see their figure 9), with errors naturally increasing for fainter and more distant galaxies. However a comparison with faint spectroscopic samples obtained in the COSMOS field (Lilly et al. 2007) revealed a dispersion $\sigma_{\Delta z/(1+z)}$ as low as 0.06 for sources with $23\,\mathrm{mag} < i^{+}_{\mathrm{AB}} < 25\,\mathrm{mag}$ at $1.5 \lesssim z \lesssim 3$. These small uncertainties will be critical for our analysis of the MIPS-selected galaxy population given the large fraction of $24\,\mu$m sources associated with faint (i.e., $i^{+}_{\mathrm{AB}} \gtrsim 24$ mag) optical counterparts at $z \gtrsim 1$.

The redshifts provided by I09 were determined using a library of star-forming and passive galaxy templates and they are not adapted to galaxies dominated in their optical/near-IR continuum by the contribution of an active galactic nucleus (such as the type 1 AGNs and optically-luminous quasars). This issue must be treated with care given the non-negligible contribution of AGNs to IR-selected galaxy samples (e.g., Genzel et al. 1998; Houck et al. 2005). The redshifts of the $24\,\mu$m sources also identified with an X-ray counterpart were therefore supplemented using the catalog of Salvato et al. (2009), which provides photometric redshifts for 1542 X-ray selected sources detected in the $XMM$-Newton observations of COSMOS (Hasinger et al. 2007; Brusa et al.

2007). Salvato et al. (2009) used an optimized set of templates with hybrid combinations of AGN and non-active galaxy SEDs, which allowed them to derive photometric redshifts with an accuracy comparable to that achieved by Ilbert et al. (2009). They also made an extensive use of multi-epoch observations of COSMOS to correct for the time-variability of type 1 AGNs. The photometric redshifts of the full $XMM$-selected sample mostly lie at $0.5 \lesssim z \lesssim 1.5$ but extend up to $z \sim 3$, with an accuracy as good as $\sigma_{\Delta z/(1+z)} = 0.015$ for faint sources ($i^+_{\rm AB} \gtrsim 22.5\,{\rm mag}$) at $z \sim 1$ (Salvato et al. 2009).

We stress that the redshifts of I09 were also used in the case of the $24\,\mu{\rm m}$ sources associated with obscured nuclei (such as sources characterized by a rising power-law continuum in the IRAC bands) but with no X-ray detection. Their emission at optical wavelengths is usually dominated by the contribution of their host galaxy and the photometric redshifts of I09 should not be significantly less accurate than those determined for star-forming sources. This argument is actually reinforced by the rather good agreement that we observed betweeen the redshifts of Salvato et al. (2009) and those of Ilbert et al. (2009) for the type 2 AGNs common to both samples.

### 2.3.2. *Photometric redshifts of 24 $\mu$m sources*

To derive the photometric redshifts of the $24\,\mu{\rm m}$ sources we first correlated the list of their $K_s$–band counterparts with the catalog of Ilbert et al. (2009) using a matching radius of $1''$. We found a single optical counterpart at $i^+_{\rm AB} < 26.5\,{\rm mag}$ for $35\,347$ $K_s$–band sources (90% of the full $24\,\mu{\rm m}$ source catalog). Double matches were obtained for 361 other $K_s$–band objects. In those cases, we noticed that the difference between the matching distances of the first and the second closest matches was large enough to consider the first one as the most likely optical counterpart. The catalog of I09 is limited to $i^+_{\rm AB} = 26.5\,{\rm mag}$ and no optical match could be found for the remaining $1\,855$ $K_s$–band sources (i.e., $i^+_{\rm AB} > 26.5\,{\rm mag}$).

From this match between the $K_s$ and the optical bands we then identified $1\,129$ optical counterparts also associated with a source detected by $XMM$. Among those, $1\,111$ are included in the analysis presented by Salvato et al. (2009) and we thus assigned to these objects the photometric redshifts provided in their catalog of X-ray sources. The identification of the optical counterparts associated with the remaining 18 $XMM$ objects is considered less secure (Brusa et al. 2007). For these objects we kept the original photometric redshift derived by I09.

Finally we considered the list of the $1\,797$ MIPS-$24\,\mu{\rm m}$ sources for which we did not find any $K_s$–band counterpart (see Sect. 2.2). We correlated this list with the catalog of Ilbert et al. (2009) using a matching radius of $2''$, assuming that some of these sources could have counterparts detected in the very deep Subaru $i^+$–band observations of COSMOS (Taniguchi et al. 2007) but not reported in our $K_s$–band catalog. Among these $24\,\mu{\rm m}$ sources, 667 objects were identified with one single counterpart in the optical catalog. We note that some of them seem qto be trully detected in the $K_s$–band image of COSMOS (McCracken et al.), although their associated signal to noise is very low. As previously reported

some of them also have counterparts at $3.6\,\mu{\rm m}$ in the IRAC data. These "by-eye" detections gave us further confidence in the reliability of their identification in the $i^+$–band catalog of I09.

To summarize, we derived photometric redshifts for $\sim 92\%$ objects of the initial $24\,\mu{\rm m}$ catalog selected above $60\,\mu{\rm Jy}$. Sources with counterparts in the $K_s$–band but no identification at $i^+_{\rm AB} < 26.5\,{\rm mag}$ account for a fraction of 5%, while 3% of the catalog correspond to $24\,\mu{\rm m}$ sources with no identification in the optical nor in the near-IR. If we rather consider a selection above $80\,\mu{\rm Jy}$, we find a total of $29\,410$ sources in the initial MIPS-$24\,\mu{\rm m}$ catalog and 94% of these objects are identified with a redshift. Independently of their possible association with a $K_s$–band or $3.6\,\mu{\rm m}$ counterpart, the $24\,\mu{\rm m}$ sources with no redshift are very faint at optical wavelengths. Previous studies have shown that they mostly correspond to highly-obscured luminous galaxies at $1 \lesssim z \lesssim 3$ rather than low redshift sources populating the faint end of the luminosity function (e.g., Houck et al. 2005; Dey et al. 2008).

### 2.3.3. *Characterization of the photometric redshift uncertainties*

By construction an infrared-selected sample of sources is biased toward dusty galaxies. The determination of photometric redshifts for these objects is subject to more uncertainties if the effect of dust extinction is not properly taken into account. Furthermore, a large fraction of mid-IR sources in the distant Universe are associated with very faint optical counterparts also characterized by less accurate redshifts. The uncertainties affecting the photometric redshifts of the COSMOS MIPS-$24\,\mu{\rm m}$ sources should thus be carefully assessed before analyzing our sample further.

Ilbert et al. (2009) presented a detailed comparison between their photometric redshifts and the spectroscopic redshifts of MIPS-$24\,\mu{\rm m}$ sources determined by Lilly et al. (2007) and Kartaltepe et al. (in prep.) with spectroscopic follow-ups of the COSMOS field. Up to $z \sim 1.5$ I09 found median dispersions $\sigma_{\Delta z/(1+z)}$ as low as 0.01 and 0.05 for $24\,\mu{\rm m}$ sources with $22.5\,{\rm mag} < i^+_{\rm AB} < 24\,{\rm mag}$ and $24\,{\rm mag} < i^+_{\rm AB} < 25\,{\rm mag}$ respectively. For mid-IR galaxies at higher redshifts and/or with fainter optical counterparts there is however no spectroscopic sample currently available in COSMOS to allow such comparison. To characterize the uncertainties of their photometric redshifts we relied on their associated Probability Distribution Functions PDF(z) as provided by I09. For their optically-selected sample Ilbert et al. (2009) showed that the $1\sigma$ uncertainties[15] derived from these PDF(z) provide a reliable estimate of the dispersion $\sigma_{\Delta z/(1+z)}$ obtained from the comparison with spectroscopic redshifts. In Figure 2 we show these $1\sigma$ uncertainties restricted to the MIPS-$24\,\mu{\rm m}$ sources as a function of their photometric redshifts, along with their median value calculated in three different bins of $i^+$–band magnitude. Up to

---

[15] Here we define the positive $1\sigma^+$ and negative $1\sigma^-$ photometric redshift uncertainties using the relation $\chi^2(z_{\rm best} + 1\sigma^+) = \chi^2(z_{\rm best} - 1\sigma^-) = min(\chi^2(z)) + 1$, with $z_{\rm best}$ the most likely photometric redshift estimated from the minimum of the merit function $\chi^2(z)$. For each object the final $1\sigma$ uncertainty is taken as the maximum between $1\sigma^+$ and $1\sigma^-$.

the highest redshift bins characterizing our sample (i.e., $z \lesssim 3$) we see that the photometric redshifts are still quite robust up to $i^+_{AB} < 25 \, \text{mag}$ ($1\sigma \lesssim 0.15$). At fainter magnitudes, the uncertainties are somehow larger but the dispersions are still as low as $1\sigma \lesssim 0.25$ up to $z \sim 2$ where most of the faint sources in our sample are located (see Sect. 3).
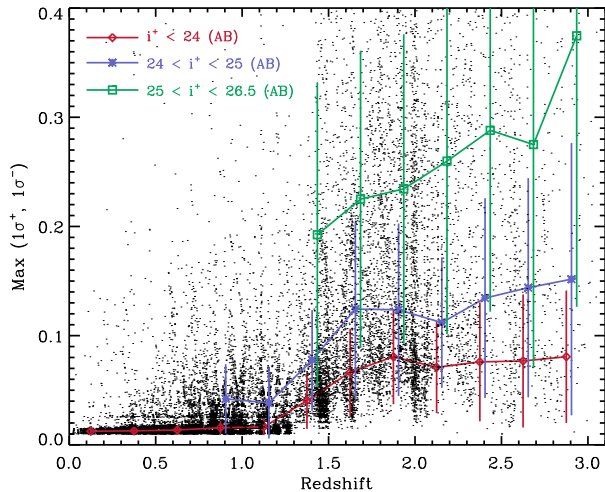


FIG. 2.— Photometric redshift uncertainties ($\sim 1\,\sigma$) of the COSMOS $24\,\mu\text{m}$–selected sources with $S_{24\mu\text{m}} > 80\,\mu\text{Jy}$ (dots), estimated using the probability distribution functions of Ilbert et al. (2009) and represented as a function of photometric redshift. The solid lines represent the median values calculated in three bins of $i^+$–band magnitude (open diamonds: $i^+ < 24$ mag; asterisks: $24 \, \text{mag} < i^+ < 25 \, \text{mag}$; open squares: $25 \, \text{mag} < i^+ < 26.5 \, \text{mag}$) and using at least 50 sources per bin of redshift. The associated error bars were computed from the median absolute deviation of each underlying distribution. [*See the electronic edition of the Journal for a color version of this figure.*]



FIG. 3.— Fraction of $24\,\mu\text{m}$ sources with $S_{24\mu\text{m}} > 80\,\mu\text{Jy}$ and characterized by a redshift probability distribution function with two different peaks, illustrated as a function of redshift for the same bins of $i^+$–band magnitude as those considered in Figure 2 (top panel). Each value was estimated using at least a total of 10 sources per bin of redshift and $i^+$–band magnitude. Error bars were computed from Poissonian uncertainties. The bottom panel shows the redshift distributions of the $24\,\mu\text{m}$ sources associated with counterparts at $24 \, \text{mag} < i^+ < 25 \, \text{mag}$ (light grey shaded region) and $25 \, \text{mag} < i^+ < 26.5 \, \text{mag}$ (dark grey shaded region). Note the very small fraction of outliers up to $z \sim 2.5$. The increasing trend observed at $i^+ > 24$ mag and $0.8 \lesssim z \lesssim 1.3$ affects only a relatively small number of sources. [*See the electronic edition of the Journal for a color version of this figure.*]

The larger uncertainties that may affect the photometric redshifts of faint optical sources can be produced by the presence of multiple peaks in their PDF($z$). To quantify the contribution of these potential catastrophic failures we considered the fraction of MIPS-$24\,\mu\text{m}$ sources with a PDF($z$) showing a secondary local maximum stronger than 10% of the value of its first peak. These fractions are illustrated as a function of redshift and for different bins of optical magnitudes in Figure 3. They show that up to $z \sim 2.5$ the number of possible outliers is negligible ($\lesssim 5\%$) for most of our sample. Fractions reaching $\sim 25\%$ may be observed at $i^+_{AB} > 24$ mag and $0.8 \lesssim z \lesssim 1.3$, yet these estimates only affect a very small number of sources (see bottom panel of Figure 3).

## 3. DIFFERENTIAL SOURCE NUMBER COUNTS

The differential $24\,\mu\text{m}$ source number counts normalized to the euclidean slope and derived from our COSMOS data are shown in Figure 4. They are compared with the counts obtained by Papovich et al. (2004) based on the MIPS *Guaranteed Time Observer* programs and by Chary et al. (2004) using deep observations in the ELAIS-N1 field. Within the uncertainties our results show a quite good agreement with these two o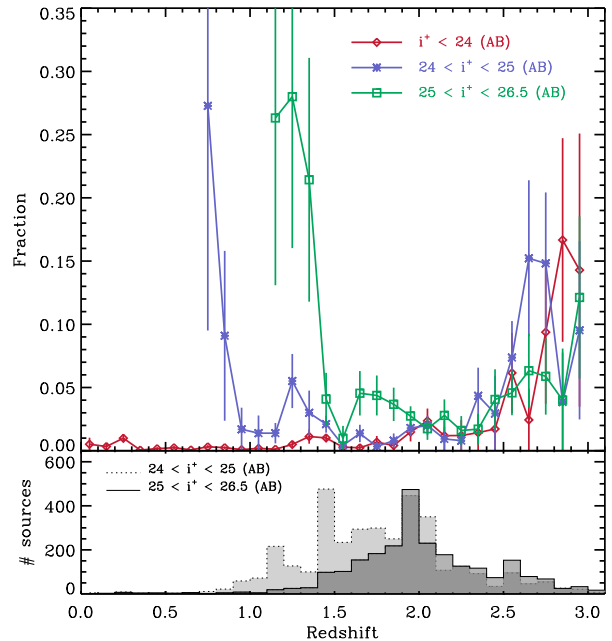ther surveys, and the variations between the three determinations may result from the effect of cosmic variance between the different fields observed with *Spitzer*. At fluxes brighter than $\sim 3 \, \text{mJy}$ though, the catalog that we derived outside of the optically-masked regions of COSMOS underestimates the density of sources compared to the counts derived over the whole area of the field. This is not surprising given that many of the $24\,\mu\text{m}$ bright objects are associated with optically-bright counterparts in these masked regions. Such objects are either stars or very low redshift galaxies, which should not affect too much our analysis of the general extragalactic $24\,\mu\text{m}$ source population.

Similar to what was observed in other *Spitzer* $24\,\mu\text{m}$ deep surveys (Marleau et al. 2004; Papovich et al. 2004; Chary et al. 2004), the counts measured from our COSMOS data show a prominent break at flux densities $S_{24\mu\text{m}} \sim 0.2$–$0.3\,\text{mJy}$. Our source extraction is highly reliable at these flux levels and this feature can not be artificially produced by an incompleteness of our $24\,\mu\text{m}$ catalog. Such a rapid "turn-over" in the euclidean-normalized source number counts implies their rapid convergence at fainter fluxes ($S_{24\mu\text{m}} \lesssim 0.1\,\text{mJy}$). Hence, a large fraction of the $24\,\mu\text{m}$ background must be produced by sources readily detected in our COSMOS MIPS data. For instance Papovich et al. (2004) assumed a straight extrapolation of the faint-end slope of the counts measured down to $S_{24\mu\text{m}} \sim 60\,\mu\text{Jy}$ and they argued that
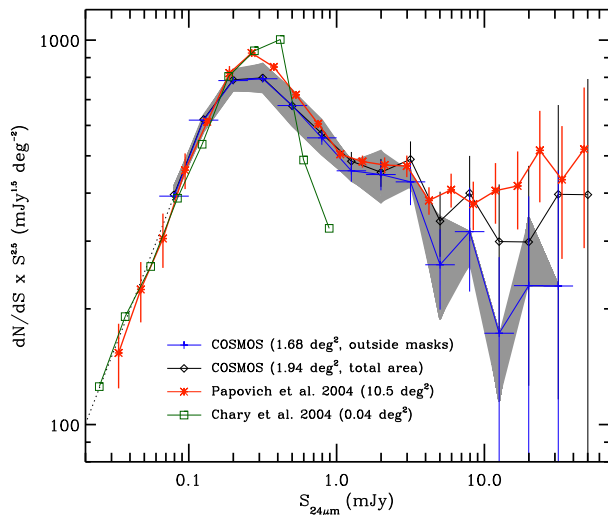
FIG. 4.— Differential $24\,\mu$m source number counts derived from the COSMOS field outside of the optically-masked regions ('plus' symbols). The grey shaded area illustrates the effect of adding a systematic uncertainty of $\pm 5\%$ to the absolute $24\,\mu$m flux calibration. The counts derived for the full coverage of COSMOS (open diamonds) as well as the counts from Papovich et al. (2004, asterisks) and Chary et al. (2004, open squares) are shown for comparison. Our error bars only take into account the statistical Poisson uncertainties. Our selection outside the masked regions is mostly complete for sources at $80\,\mu$Jy $\lesssim$ S$_{24\mu m} \lesssim 3$ mJy. The dotted line shows our extrapolation of the COSMOS source number counts at fluxes below $80\,\mu$Jy (see Sect. 5). [*See the electronic edition of the Journal for a color version of this figure.*]

MIPS-$24\,\mu$m sources detected above $60\,\mu$Jy resolve as much as $\sim 70\%$ of the $24\,\mu$m background intensity. In Sect. 5 we will use our photometric redshift identifications in COSMOS to explore the build-up of this mid-IR background light *as a function of cosmic time.*

Finally, we note that the persistent "shoulder" appearing at $S_{24\mu m} \sim 3$ mJy in the normalized counts that were derived from large area surveys such as the *Spitzer Wide-Area Infrared Extragalactic Survey* (SWIRE, Shupe et al. 2008) is also visible in COSMOS (although our data alone can not formally exclude an effect of cosmic variance). To our knowledge this characteristics of the $24\,\mu$m counts has not been explained so far.

## 4. OBSERVED REDSHIFT DISTRIBUTIONS

We now explore the redshift distribution of the COS-MOS MIPS-$24\,\mu$m sources based on the identifications of their photometric redshifts described in Sect. 2.3. We define $\mathcal{H}_{24}(z, i^+_{\rm lim}, S^{24\mu m}_{\rm lim})$ the redshift distribution of the $24\,\mu$m–selected sources with $S_{24\mu m} > S^{24\mu m}_{\rm lim}$ and associated with optical counterparts at $i^+ < i^+_{\rm lim}$, and we note $\mathcal{H}_{\rm opt}(z, i^+_{\rm lim})$ the redshift distribution of all the COS-MOS optically–selected sources with $i^+ < i^+_{\rm lim}$. Given the relatively small number of AGN-dominated sources in the general population of optically-selected galaxies[16], $\mathcal{H}_{\rm opt}(z, i^+_{\rm lim})$ was computed directly using the photometric redshift catalog of Ilbert et al. (2009). In Figure 5

---

[16] Only 0.8% of optical sources with $i^+ < 24$ mag are detected in the $XMM$ observations of COSMOS down to F$_{0.5-2\,\rm keV} \sim 5 \times 10^{-16}$ erg cm$^{-2}$ s$^{-1}$.

we show the redshift distributions $\mathcal{H}_{24}(z, i^+_{\rm lim}, S^{24\mu m}_{\rm lim})$ cal-culated down to flux limits of $80\,\mu$Jy and $300\,\mu$Jy at $24\,\mu$m and for $i^+$–band magnitudes limits of 24, 25 and 26.5 mag. Sources brighter than $i^+_{\rm AB} = 20$ mag were ex-cluded from all these estimates to minimize the effect of large scale structures at low redshift. Our redshift distri-bution at $z \lesssim 0.4$ should actually be treated with caution given the limited comoving volume sampled by our sur-vey at these small distances.

We see that to the depth of our MIPS observa-tions ($S_{24\mu m} > 80\,\mu$Jy) almost all $24\,\mu$m sources at $z \lesssim 1$ are associated with optical counterparts brighter than $i^+_{\rm AB} \sim 24$ mag. Our photometric redshifts are very ac-curate at these optical magnitudes. Given the statis-tics of our sample beyond $z \sim 0.5$ our redshift distribu-tions at $0.5 \lesssim z \lesssim 1$ should thus be highly robust indepen-dently of the $24\,\mu$m flux limit considered above $80\,\mu$Jy. At $z \gtrsim 1$, the contribution of fainter sources becomes more significant. For instance, 45% and 33% of the MIPS-$24\,\mu$m sources with respectively $S_{24\mu m} > 80\,\mu$Jy and $S_{24\mu m} > 300\,\mu$Jy at $z > 1$ are associated with coun-terparts fainter than $i^+_{\rm AB} = 24$ mag. As we showed in Sect. 2.3 their photometric redshifts are still quite reli-able though (see Figures 2 & 3).

Our redshift distribution estimates are mainly affected by the errors on the COSMOS photometric redshifts, the cosmic variance and the errors on the $24\,\mu$m flux densi-ties. To quantify the impact of all these uncertainties we first divided the COSMOS field into 4 different regions of similar areas ($\sim 0.4\,\rm deg^2$) and we derived the possible range of redshift distributions in each region with a set of 5 000 Monte Carlo simulations. For each of these sim-ulations we considered our *full* $24\,\mu$m catalog down to $S_{24\mu m} = 60\,\mu$Jy and we modified the $24\,\mu$m flux and red-shift of each single source according to their $24\,\mu$m flux uncertainty and their $1\sigma$ photometric redshift dispersion characterized in Sect. 2. Assuming a given $24\,\mu$m flux limit, an average and independent redshift distribution was estimated for the 4 different regions and the disper-sion between these 4 estimates was taken as the final un-certainty affecting the global $24\,\mu$m source redshift distri-bution. Our different estimates are reported in Table 1. They are also shown in the bottom panels of Figure 5 for $24\,\mu$m flux limits of $80\,\mu$Jy and $300\,\mu$Jy. They sug-gest that our global redshift distributions inferred from the $1.68\,\rm deg^2$ area observed with MIPS should be robust within $\sim 20\%$ up to $z \sim 3$.

It is important to note that the redshift distribution characterizing the galaxy population selected in the mid-IR differs quite significantly from the one observed at op-tical wavelengths. Figure 6 illustrates how the optically and mid-IR selected sources differ in their occupation of the redshift/$i^+$–band magnitude parameter space. For instance we find that only $\sim 27\%$ of the optically-selected galaxies with $i^+_{\rm AB} < 24$ mag are located at $z \gtrsim 1$ (Ilbert et al. 2009) while this fraction rises to more than 50% for the $24\,\mu$m sources with $S_{24\mu m} > 80\,\mu$Jy. This large proportion of high-redshift mid-IR galaxies is mostly lo-cated at $1 \lesssim z \lesssim 2.5$ and it has already been seen in other MIPS high redshift surveys (e.g., Houck et al. 2005; Yan et al. 2005; Caputi et al. 2006; Papovich et al. 2007; De-sai et al. 2008). It results primarily from the strong evo-lution that infrared–luminous galaxies have undergone
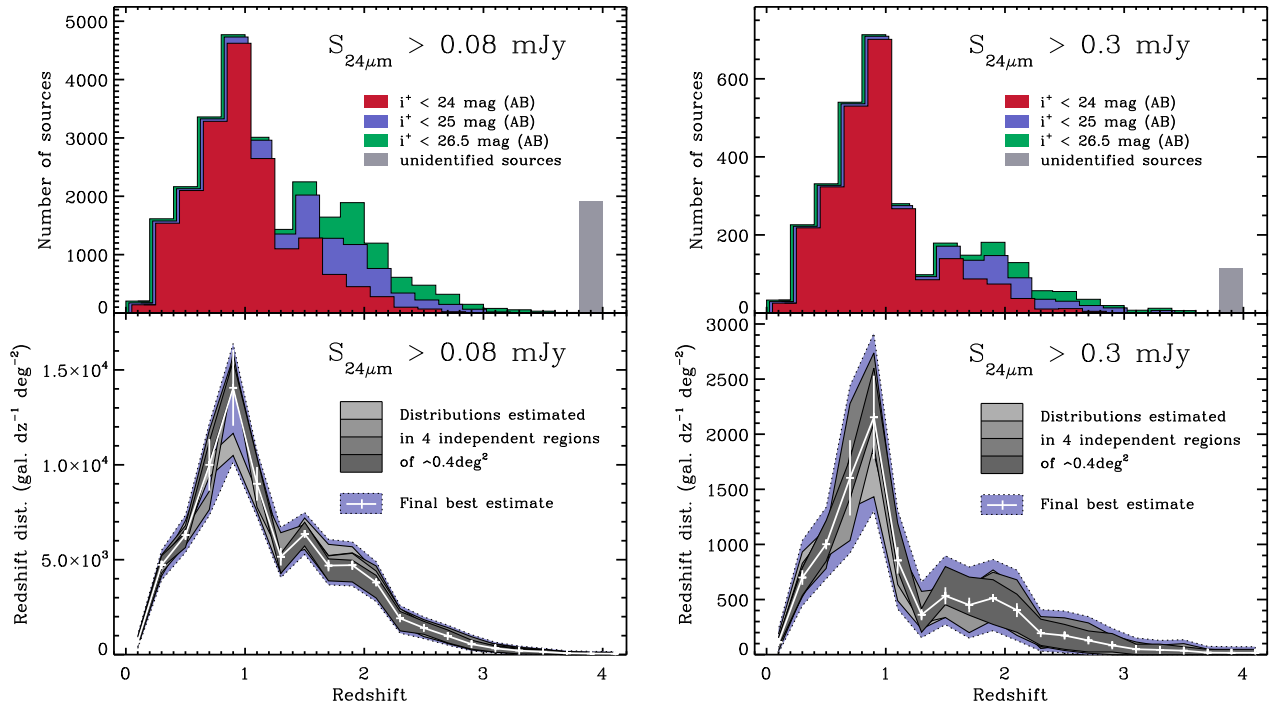
FIG. 5.— Redshift distributions $\mathcal{H}_{24}(z, i_{\text{lim}}^+, S_{\text{lim}}^{24\mu\text{m}})$ of $24\,\mu\text{m}$ sources with $S_{\text{lim}}^{24\mu\text{m}} = 80\,\mu\text{Jy}$ (left) and $S_{\text{lim}}^{24\mu\text{m}} = 300\,\mu\text{Jy}$ (right). The top panels represent the redshift histograms determined for different cuts of $i_{\text{AB}}^+$–band magnitude as indicated by each legend. The contribution of objects with no redshift ($i_{\text{AB}}^+ > 26.5\,\text{mag}$) is represented as a single bin on the right hand side of the diagrams. The bottom panels show our final and best estimates of $\mathcal{H}_{24}(z, S_{\text{lim}}^{24\mu\text{m}})$ along with their corresponding $1\sigma$ uncertainties (white solid lines). They were derived from the range of possible redshift distributions defined by the dotted lines and obtained after accounting for the effect of cosmic variance and Poissonian uncertainties. The variance produced by large scale structures was quantified by computing the redshift distributions in 4 different $\sim0.4\,\text{deg}^2$ regions of COSMOS and with Monte-Carlo simulations accounting for the flux and redshift uncertainties of the MIPS sources (grey shaded areas). Galaxies brighter than $i_{\text{AB}}^+ = 20\,\text{mag}$ were excluded from all samples to minimize the cosmic variance fluctuations at low redshift. [*See the electronic edition of the Journal for a color version of this figure.*]

with time (e.g., Blain et al. 1999; Franceschini et al. 2001; Chary & Elbaz 2001). Given the broad-band aromatic features commonly observed at $6\,\mu\text{m} \lesssim \lambda \lesssim 20\,\mu\text{m}$ in the spectra of star-forming galaxies it may also be due to galaxy $k$-corrections boosting the mid-IR detectability of sources at $1.5 \lesssim z \lesssim 2.5$ when these features are redshifted into the MIPS-$24\,\mu\text{m}$ bandpass (e.g., Lagache et al. 2004).

To better characterize this large contribution of mid-IR selected sources at high redshift, we considered the relative distribution $\mathcal{H}_{24}(z, i_{\text{lim}}^+, S_{\text{lim}}^{24\mu\text{m}})/\mathcal{H}_{\text{opt}}(z, i_{\text{lim}}^+)$. First, this quantity allows us to check if any feature of the MIPS-$24\,\mu\text{m}$ galaxy redshift distribution does not artificially result from a bias already present in the underlying optically–selected catalog of photometric redshifts. Besides, it can be seen as the fraction of optical sources with $i^+ < i_{\text{lim}}^+$ and with a mid-IR detection above a $24\,\mu\text{m}$ flux limit $S_{\text{lim}}^{24\mu\text{m}}$. Our different estimates of $\mathcal{H}_{24}/\mathcal{H}_{\text{opt}}$ are illustrated in the bottom panels of Figure 6 for the same $24\,\mu\text{m}$ flux and $i^+$–band magnitude limits as the ones considered previously. We see that independently of these limits the fraction of optical sources detected in the mid-IR progressively rises with redshift, which must be related to the well-known increase of star formation density with lookback time. The fraction peaks at $z \sim 2$ before gradually declining at higher redshifts, probably because of the decreasing number of $24\,\mu\text{m}$ detections at

$z \gtrsim 2$.

More interestingly though, we observe a substantial drop of $\mathcal{H}_{24}/\mathcal{H}_{\text{opt}}$ between $z \sim 1$ and $z \sim 1.3$ followed by a steep increase from $z \sim 1.3$ and $z \sim 2$. This effect is clearly apparent even with a cut at $i^+ < 24\,\text{mag}$. Therefore it can not originate from systematics affecting our photometric redshifts. It is rather due to the break characterizing the $24\,\mu\text{m}$ source redshift distributions around $z \sim 1.3$ and that does not appear in the smooth distributions observed at optical wavelengths (e.g., I09). Note that this break also seems to be more prominent as the $24\,\mu\text{m}$ flux limit increases. The redshift distribution derived at $S_{24\mu\text{m}} > 300\,\mu\text{Jy}$ looks even like a two-component function with a main and narrow peak of sources at $z \sim 1$ followed by a secondary but broader peak at $1.5 \lesssim z \lesssim 2.5$ (e.g., Figure 5, right panel). This characteristic of the $24\,\mu\text{m}$ redshift distribution could be artificially produced by a relative increase of mid-IR detections at $z \sim 2$ due to the rest-frame $7.7\,\mu\text{m}$ aromatic feature enhancing the apparent $24\,\mu\text{m}$ flux of star-forming galaxies when it is redshifted into the MIPS-$24\,\mu\text{m}$ bandpass. On the other hand it may also reflect a smaller rate of detections at $z \sim 1.3$ given the possible effect of the $9.7\,\mu\text{m}$ silicate absorption. If this break is trully produced by $k$-correction effects, the stronger effect observed at brighter $24\,\mu\text{m}$ flux might also suggest more prominent features in the more luminous mid-IR selected galaxies.

TABLE 1
Redshift distributions of the COSMOS MIPS-24 $\mu$m selected sources [a]

| Redshift | N(z, $S_{24} > 0.08$ mJy) | N(z, $S_{24} > 0.15$ mJy) | N(z, $S_{24} > 0.3$ mJy) |
|---|---|---|---|
| $0.0 < z < 0.2$ | $679 \pm 91$ | $310 \pm 63$ | $110 \pm 20$ |
| $0.2 < z < 0.4$ | $4722 \pm 203$ | $2356 \pm 64$ | $697 \pm 62$ |
| $0.4 < z < 0.6$ | $6317 \pm 275$ | $3296 \pm 71$ | $997 \pm 44$ |
| $0.6 < z < 0.8$ | $9991 \pm 1328$ | $4964 \pm 796$ | $1604 \pm 353$ |
| $0.8 < z < 1.0$ | $14055 \pm 2001$ | $7144 \pm 1193$ | $2148 \pm 377$ |
| $1.0 < z < 1.2$ | $8981 \pm 904$ | $3743 \pm 471$ | $865 \pm 117$ |
| $1.2 < z < 1.4$ | $5158 \pm 465$ | $1704 \pm 167$ | $367 \pm 54$ |
| $1.4 < z < 1.6$ | $6360 \pm 144$ | $2356 \pm 155$ | $531 \pm 78$ |
| $1.6 < z < 1.8$ | $4672 \pm 288$ | $1993 \pm 117$ | $452 \pm 67$ |
| $1.8 < z < 2.0$ | $4735 \pm 264$ | $2167 \pm 203$ | $497 \pm 30$ |
| $2.0 < z < 2.2$ | $3753 \pm 203$ | $1683 \pm 150$ | $411 \pm 62$ |
| $2.2 < z < 2.4$ | $1933 \pm 65$ | $815 \pm 52$ | $205 \pm 13$ |
| $2.4 < z < 2.6$ | $1423 \pm 93$ | $598 \pm 51$ | $167 \pm 27$ |
| $2.6 < z < 2.8$ | $978 \pm 110$ | $406 \pm 54$ | $126 \pm 31$ |
| $2.8 < z < 3.0$ | $535 \pm 89$ | $222 \pm 32$ | $84 \pm 21$ |
| $3.0 < z < 3.2$ | $335 \pm 34$ | $125 \pm 8$ | $49 \pm 6$ |
| $3.2 < z < 3.4$ | $203 \pm 30$ | $103 \pm 17$ | $43 \pm 5$ |
| $3.4 < z < 3.6$ | $138 \pm 7$ | $67 \pm 14$ | $36 \pm 18$ |
| $3.6 < z < 3.8$ | $73 \pm 7$ | $42 \pm 8$ | $18 \pm 7$ |
| $3.8 < z < 4.0$ | $53 \pm 8$ | $31 \pm 9$ | $16 \pm 5$ |
| $4.0 < z < 4.2$ | $46 \pm 10$ | $34 \pm 7$ | $16 \pm 3$ |

[a] The distributions N(z) refer to the number of sources per redshift unit and per square degree. The $1\sigma$ error bars account for cosmic variance, Poisson noise, flux and redshift uncertainties as described in Sect. 4.

## 5. THE BUILD-UP OF THE MID-INFRARED BACKGROUND ACROSS COSMIC AGES

The Cosmic Infrared Background (CIB) refers to the extragalactic background light (EBL) detected between $\sim 8\,\mu$m and $\sim 1000\,\mu$m. It can be seen as a fossil record of all the radiations emitted at IR wavelengths along the process of galaxy formation (e.g., Elbaz et al. 2002). Its integrated energy power is comparable to that of the background produced by the stellar component of galaxies in the optical/near-IR wavelength range (Dole et al. 2006). Understanding how the different populations of distant sources contributed to the build-up of the CIB as a function of redshift can thus provide significant constraints to our general understanding of the cosmic growth of structures.

Using stacking analysis at $70\,\mu$m and $160\,\mu$m Dole et al. (2006) showed that $24\,\mu$m–selected sources with $S_{24\mu m} > 60\,\mu$Jy contribute more than 70% of the CIB. The large statistics available in the COSMOS field and the high rate ($\sim 95\%$) of redshift identifications in our $24\,\mu$m catalog give us therefore a unique opportunity to resolve the different contributions of galaxies to the build-up of a large fraction of the EBL. In this current paper we only explore the history of the monochromatic background light at the wavelength of our MIPS observations, using the differential $24\,\mu$m source number counts as a function of lookback time. Resolving the history of mid-IR source number counts already provides tight constraints on the different models of galaxy formation, especially when they correctly reproduce integrated measures like the total counts or the diffuse background emission but differ in their predictions of the flux/redshift distribution of galaxies responsible for these quantities. This issue will actually be discussed in Sect. 6 where we will compare our data with the predictions of different mod-

els to quantify their reliability in the description of IR galaxy evolution. We defer to a subsequent publication the analysis of the total background intensity produced by $24\,\mu$m–selected galaxies over the entire spectral range of the CIB.

To characterize this decomposition of the $24\,\mu$m counts as a function of redshift we first defined $dN(z_{\rm lim}, S_{24\mu m})/dS_{24\mu m}$ and $dN(i^+_{\rm lim}, S_{24\mu m})/dS_{24\mu m}$ the differential counts of the $24\,\mu$m sources identified up to a given redshift $z_{\rm lim}$ or up to a given $i^+$–band magnitude $i^+_{\rm lim}$, respectively. In Figure 7 we illustrate these quantities computed for $z_{\rm lim} = 0.5$, 1, 1.5, 2 and 2.5 (left panel) and for $i^+_{\rm lim} = 21$, 22, 23, 24, 25 and 26.5 mag (right panel). For comparison we also show the total number counts derived from the COSMOS field and discussed in Sect. 3 (see also Figure 4). We see that the brightest $24\,\mu$m sources are mostly associated with low redshift galaxies characterized by bright optical counterparts. However a non-negligible fraction of the MIPS detections at $S_{24\mu m} \gtrsim 1$ mJy are also located at much larger distances. Albeit rare in space density, these sources compose the bright end of the IR luminosity function at high redshift and an accurate estimate of their contribution can only be determined with large area surveys. At fainter fluxes, we also note that a substantial fraction of the $24\,\mu$m sources are associated with faint and distant optical counterparts at $i^+_{\rm AB} > 24$ mag. This conclusion reinforces that discussed above for the redshift distributions. It emphasizes once again the difficulties to achieve a complete characterization of the $24\,\mu$m-selected galaxy population with current optical/near-IR follow-ups, and in particular to obtain a full census of the sources at $S_{24\mu m} \lesssim 0.5$ mJy making the bulk of the mid-IR background light. At such faint optical magnitudes, spectroscopy has been very challenging so far while photometric redshifts also need to be carefully treated given the
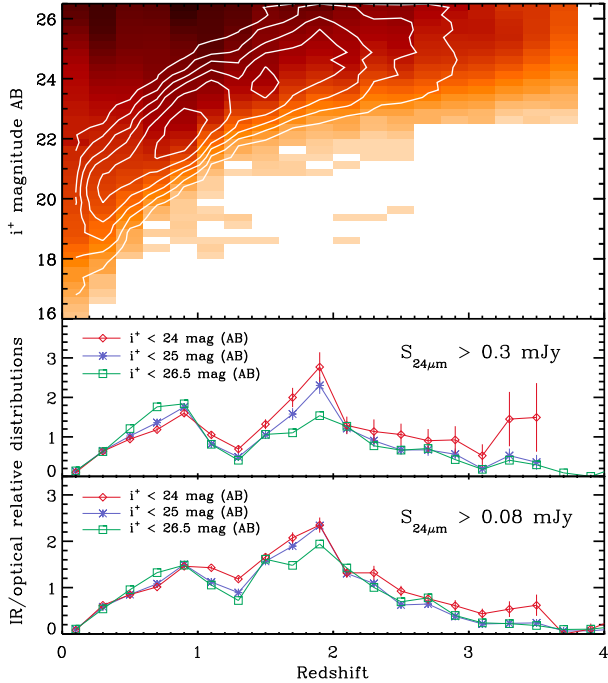
Fig. 6.— The top panel shows the distribution of $i^+$–band magnitudes as a function of redshift computed for the COSMOS $i^+$–band selected galaxies (Ilbert et al. 2009, shaded region, darkness increasing with source density) and the $24\,\mu m$ sources with $S_{24\mu m} > 80\,\mu Jy$ (white contours). The two other panels illustrate the normalized relative distributions $\mathcal{H}_{24}(z, i^+_{lim}, S^{24\mu m}_{lim})/\mathcal{H}_{opt}(z, i^+_{lim})$ for $i^+_{lim} = 24$ mag (open diamonds), $i^+_{lim} = 25$ mag (asterisks) and $i^+_{lim} = 26.5$ mag (open squares), with $\mathcal{H}_{opt}(z, i^+_{lim})$ the redshift distribution of the optically-selected sources with $i^+_{AB} < i^+_{lim}$ derived by Ilbert et al. (2009). They were computed for $S^{24\mu m}_{lim}$ of 0.3 mJy and 0.08 mJy (middle and bottom panels, respectively). The fraction of optical sources detected at $24\,\mu m$ is clearly rising up to $z \sim 2$, although a prominent break is visible at $z \sim 1.3$. [See the electronic edition of the Journal for a color version of this figure.]

rapid increase of their uncertainties beyond $I \sim 25$ mag (e.g., I09).

To also account for the contribution of galaxies fainter than our $24\,\mu m$ detection limit we extrapolated the $24\,\mu m$ number counts at faint fluxes following the same approach as considered by Papovich et al. (2004). We used power-law functions $dN/dS_{24\mu m} \propto S_{24\mu m}^{-\alpha}$ for the full $24\,\mu m$ catalog and for the different sub-samples of $24\,\mu m$ sources selected per bin of redshift or $i^+$–band magnitude as described above. For each of these extrapolations the power-law index $\alpha$ was only constrained with the counts observed above $S_{24\mu m} = 80\,\mu Jy$ to minimize the impact of the incompleteness of our source extraction below this limit. For the total counts we derived $\alpha \sim 1.5$. This is similar to the results obtained by Papovich et al. (2004), Chary et al. (2004) and Rodighiero et al. (2006) who measured indexes between 1.5 and 1.6 using sources detected down to $\sim 30\,\mu Jy$ in the ELAIS-N1 field. This good agreement suggests that the extrapolations obtained for the other sub-samples should also provide a fair representation of the flux and redshift distributions characterizing the MIPS sources below our detection limit at $24\,\mu m$.

Finally, we integrated the total extrapolated number

counts to estimate the total $24\,\mu m$ background light (referred as $B_{tot}$ hereafter). We also integrated the extrapolated functions $dN/dS_{24\mu m} \times S_{24\mu m}$ for each sub-sample considered above to define

$$B_{24\mu m}(z_{lim}, S_{24\mu m}) = \int_{S_{24\mu m}}^{\infty} dN(z_{lim}, S)/dS \times S \times dS$$
(1)

and

$$B_{24\mu m}(i^+_{lim}, S_{24\mu m}) = \int_{S_{24\mu m}}^{\infty} dN(i^+_{lim}, S)/dS \times S \times dS$$
(2)

as the background light produced above a $24\,\mu m$ flux $S_{24\mu m}$ and up to the redshift $z_{lim}$ (Eq. 1) or by sources brighter than the $i^+$–band magnitude $i^+_{lim}$ (Eq. 2)[17].

These two quantities are respectively illustrated in Figures 8 & 9 for $24\,\mu m$ fluxes of 0.06, 0.08, 0.15, 0.3 and 1 mJy as well as for $S_{24\mu m} = 0$. They were normalized to the total $24\,\mu m$ background intensity $B_{tot}$ determined from the extrapolation of the total source number counts. They can thus be read as the fraction of the $24\,\mu m$ background resolved by MIPS-selected sources as a function of their flux $S_{24\mu m}$, their redshift and their optical magnitude. The bottom panel of Figure 9 also illustrates the *differential* $24\,\mu m$ background intensity produced as a function of redshift and computed for the same $24\,\mu m$ fluxes as in the upper panel. Note that because of the magnitude limit imposed by our optical counterpart identifications $B_{24\mu m}(i^+_{lim}, S_{24\mu m})$ was only computed up to $i^+ = 26.5$ mag. Furthermore our determination of $B_{24\mu m}(z_{lim}, S_{24\mu m})$ is necessarily underestimated at high redshift given the incompleteness of our identifications at faint fluxes. However we believe that these two effects should affect our results by at most 10% given our estimate of $B_{24\mu m}(i^+_{lim}, S_{24\mu m})/B_{tot} \sim B_{24\mu m}(z_{lim}, S_{24\mu m})/B_{tot} \sim 0.9$ for $S_{24\mu m} = 0$, $i^+_{lim} = 26.5$ and $z_{lim} \to \infty$.

While mid-IR shallow surveys (e.g., $S_{24\mu m} \gtrsim 0.3\,mJy$) only resolve up to $\sim 30\%$ of $B_{tot}$ the analysis of Figures 8 & 9 reveals that the MIPS-$24\,\mu m$ sources brighter than $S_{24\mu m} \sim 60\,\mu Jy$ resolve up to $\sim 70\%$ of the total $24\,\mu m$ background. This estimate is consistent with that of Papovich et al. (2004) but it is slightly higher than the results obtained by Rodighiero et al. (2006) in the ELAIS-N1 field. Since a non-negligible fraction of the background is produced by bright sources (e.g., $\gtrsim 10\%$ at $S_{24\mu m} \gtrsim 1\,mJy$) this disagreement could be simply explained by the small area of the sky covered in their analysis ($\sim 185\,arcmin^2$) and the small number of bright $24\,\mu m$ detections in their data. Furthermore up to $\sim 10\%$ of the $24\,\mu m$ background originates from optical sources fainter than the limit of our photometric redshift catalog ($i^+ = 26.5$ mag), but more than 50% of $B_{tot}$ is due to sources detected above $80\,\mu Jy$ at $z \lesssim 1.5$ and associated with optical counterparts brighter than $i^+ = 24$ mag. Although their contribution to the integrated CIB would

_____

[17] The spectral slope of the counts at faint fluxes guarantees the convergence of the integrals when $S_{24\mu m} \to 0$ whatever the choice of the redshift or the $i^+$–band magnitude limit.

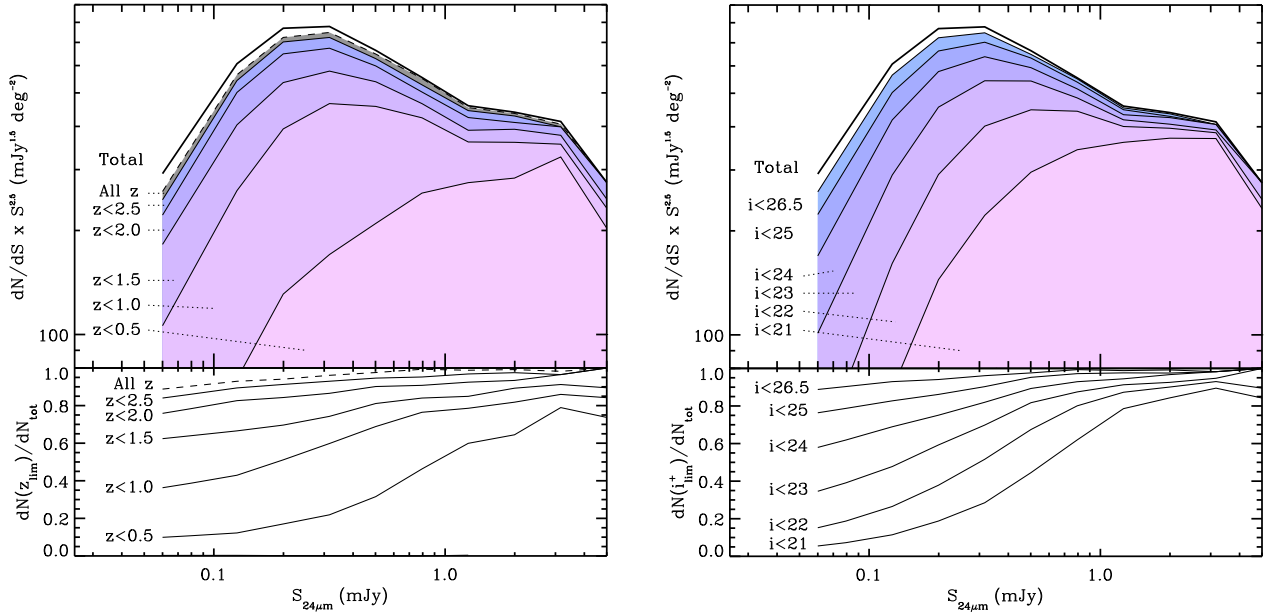FIG. 7.— Differential MIPS-24 $\mu$m number counts along with the contributions of 24 $\mu$m sources computed for different cuts in redshift (left panel) or $i^+$–band magnitude (right panel) and as shown by the shaded regions. The thick black curve represents the total number counts derived from the whole 24 $\mu$m catalog. The bin denoted as "All z" in the left panel corresponds to all 24 $\mu$m sources identified with a redshift in our survey. The corresponding fractions of sources observed in the different bins of selection are illustrated as a function of 24 $\mu$m flux density in the bottom panels. Note the increasing contribution of optically-faint ($i^+_{AB} > 24$ mag) and high-redshift galaxies to the source number counts at faint 24 $\mu$m fluxes. [*See the electronic edition of the Journal for a color version of this figure.*]

require a careful analysis of their SED in the far-IR, our picture is therefore broadly consistent with previous claims supporting a large contribution of infrared-luminous galaxies at $0.5 \lesssim z \lesssim 1.5$ to the EBL (e.g., Elbaz et al. 2002; Dole et al. 2006). Conversely, we also find that up to $\sim 30\%$ of the total 24 $\mu$m background must be produced by optically-faint ($i^+ > 24$ mag) galaxies at $z \gtrsim 1$. The exact redshift distribution of these sources can not be constrained with our data given our 24 $\mu$m flux limit of 80 $\mu$Jy as well as the incompleteness of our redshift determinations at faint 24 $\mu$m fluxes. However, the flattening of $B_{24\mu m}(z_{lim}, S_{24\mu m})$ observed in Figure 9 suggests that they should be mostly located at $1 \lesssim z \lesssim 3$.

Finally, the bottom panel of Figure 9 reveals that the relative contribution of galaxies to the 24 $\mu$m background increases up to $z \sim 1$ and rapidly declines at higher redshift. Although this trend clearly depends on our extrapolations of the counts below 80 $\mu$Jy it is again consistent with the picture suggested by phenomenological models of IR galaxy evolution (e.g. Chary & Elbaz 2001; Franceschini et al. 2001) and by the analysis of the history of the CIB recently performed with other methods (e.g., Dole et al. 2006). Nonetheless, the contribution of galaxies with $S_{24\mu m} > 80$ $\mu$Jy seems to be roughly constant up to $z \sim 1$. Hence, the "peak" observed at $z \sim 1$ must be produced by a strong evolving (albeit not dominant) contribution of galaxies fainter than 80 $\mu$Jy and with rather low infrared luminosities.

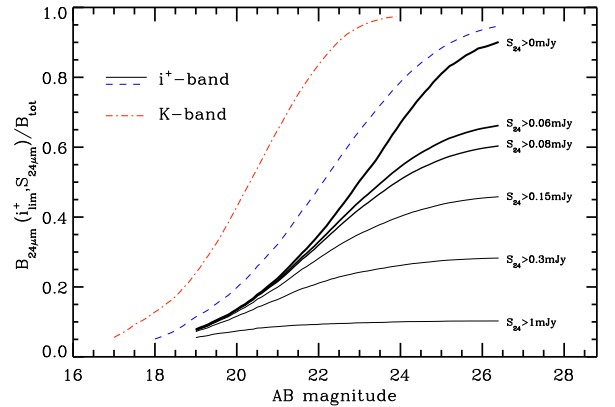## 6. COMPARISON WITH MODEL PREDICTIONS

### 6.1. *Semi-analytical models*



FIG. 8.— Fraction of the *total* 24 $\mu$m background produced by sources brighter than the $i^+$–band magnitude $i^+_{lim}$ (black thick solid line, assuming an extrapolation of the counts at the faint end), along with the fractions resolved above 24 $\mu$m fluxes of 0.06, 0.08, 0.15, 0.3 and 1 mJy (solid lines, increasing thickness corresponding to fainter flux limits). For comparison the blue-dashed (resp. red dash-dotted) line shows how the $i^+$–band (resp. $K_s$–band) sources contribute to the fraction of the 24 $\mu$m background produced above $S_{24\mu m} = 80$ $\mu$Jy and directly measured in our data.

Constraining the physics of galaxy formation with semi-analytical models has become over the last decade one of the major challenges of modern cosmology. Based on the now-popular cold dark matter (CDM) paradigm of structure formation (Springel et al. 2005) these models compute the evolution of the stellar content of galaxies from the hierarchical assembly of dark matter haloes, using detailed simulations to account for a variety of physical processes such as the radiative cooling and the shock-
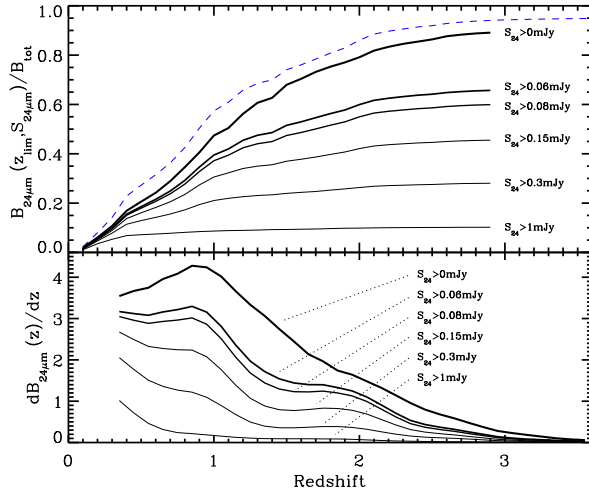
FIG. 9.— *Top:* Fraction of the *total* $24\,\mu m$ background produced by the COSMOS-selected $i^+ < 26.5$ mag sources below the redshift $z_{\rm lim}$ (black thick solid line, assuming an extrapolation of the counts at the faint end), along with the fractions resolved above $24\,\mu m$ fluxes of 0.06, 0.08, 0.15, 0.3 and 1 mJy. For comparison the blue-dashed line shows how the identified $24\,\mu m$ sources contribute to the fraction of the $24\,\mu m$ background produced above $S_{24\mu m} = 80\,\mu Jy$ and directly measured in our data. Uncertainties due to the incompleteness of our redshift identification beyond $z \sim 1$ should be at most 10%. *Bottom:* Differential background intensity (arbitrary units) produced as a function of redshift and computed with the same selection criteria as in the top panel.

heating of gas, the energy feedback from supernovae and active nuclei, the chemical enrichment of the interstellar medium and galaxy mergers (e.g., Cole et al. 2000; Bower et al. 2006; Croton et al. 2006; Cattaneo et al. 2006). Although many quantitative aspects of galaxy evolution are still not correctly predicted with these scenarios they have recently been successful in reproducing several key properties of present-day galaxies such as their large-scale clustering or the bimodality of their optical color distribution (Blaizot et al. 2006; Somerville et al. 2008).

Because of the additional difficulty to properly account for dust extinction, the determination of accurate predictions of the deep IR Universe with these models has been however barely explored so far. Simulating the evolution of galaxy IR properties requires not only a correct estimate of the history of the physical processes powering their energy output over relatively short time scales (e.g., star-forming activity, nuclear accretion), but an accurate treatment of their reprocessing of UV/optical radiation at longer wavelengths is also critical. Since the launch of *Spitzer* Lacey et al. (2008) published the only single study (to our knowledge) describing some of the expected properties of $24\,\mu m$-selected galaxies with the use of a semi-analytical model based on the hierarchical growth of dark matter haloes[18]. Their simulations were performed with the GALFORM galaxy formation model (Cole et al. 2000). They used the GRASIL spectro-photometric code (Silva et al. 1998) to calculate SEDs and to account for the reprocessing of radiation by dust, which allows for

predictions of the multi-wavelength properties of all simulated galaxies as a function of cosmic time.

Figure 10 shows their model predictions for the evolution of the galaxy median redshift as a function of $24\,\mu m$ flux, along with their estimates of the $10^{\rm th}$ and $90^{\rm th}$ percentiles characterizing the associated redshift distributions. They are compared with the same quantities estimated from our COSMOS data, where the reported error bars account for the combination of flux and redshift uncertainties, the cosmic variance and the Poisson noise as described in Sect. 4. Interestingly enough, we note that the model of Lacey et al. (2008) shows a statistically-significant overestimate of the median redshift of galaxies at all fluxes probed by our survey. This overestimate is particularly noticeable at fluxes below $\sim 0.5$ mJy. Given that their predictions agree reasonably well with the total source number counts observed at such flux levels (see their figure 2), it implies an excess of faint sources predicted above $z \sim 1$ as well as a lack of sources predicted at lower redshifts. This disagreement was already noticed by Lacey et al. (2008) from the comparison between their model and luminosity functions previously derived from *Spitzer* data. It is also clearly apparent in Figure 11, where we compare the COSMOS redshift distribution measured above $S_{24\mu m} = 83\,\mu Jy$ with the result of the simulations that they obtained for the same $24\,\mu m$ flux limit. On the other hand we also note that the $90^{\rm th}$ percentile of the distribution observed in COSMOS at bright fluxes seems to extend up to higher redshifts compared to the model predictions. This could be interpreted as an underestimate of the bright end of the simulated IR luminosity function at $1.5 \lesssim z \lesssim 2.5$. It could also be due to an excess of sources at much lower redshifts since the model of Lacey et al. (2008) overestimates the differential $24\,\mu m$ source number counts above $\sim 1$ mJy. We will investigate these different possible interpretations in future papers where we will present the IR luminosity functions derived from our MIPS imaging of the COSMOS field.

In Figures 12 and 13 we now confront the observed and the predicted distributions of $24\,\mu m$ sources as a function of their near-IR and optical photometry. Following the same selection criteria as those considered by Lacey et al. (2008) we restrict our sample to sources brighter than $S_{24\mu m} = 83\,\mu Jy$. We split these sources in different bins of $K_s$–band and $r^+$–band magnitude and we compare the redshift distributions observed in these bins with the corresponding predictions derived from the simulations[19]. The range of distributions shown for the COSMOS data (grey shaded regions) accounts for our best estimate of cosmic variance, flux and redshift uncertainties (see Sect. 4). The photometric errors affecting the $r^+$–band and $K_s$–band data were not taken into account but their effect should be limited given the adopted bins of magnitudes and the depth of the COSMOS observations ($r^+ < 26.8$ mag AB and $K_s < 23.8$ mag AB at $5\sigma$: Capak et al. 2007, McCracken et al. submitted).

As already noted by Lacey et al. (2008), our figures 12 & 13 show that the excess of simulated sources

---

[18] Silva et al. (2005) derived similar predictions based on the semi-analytical model of Granato et al. (2004), but this model does not include galaxy merging.

[19] Lacey et al. (2008) provide their predicted distributions using magnitudes in the Vega system. We thus transformed our AB magnitudes assuming $r^+_{\rm Vega} = r^+_{\rm AB} - 0.16$ and $K_{\rm s,Vega} = K_{\rm s,AB} - 1.84$. The transformation between our set of filters ($r^+$ & $K_s$) and that used by Lacey et al. ($R$ & $K$) was however neglected.
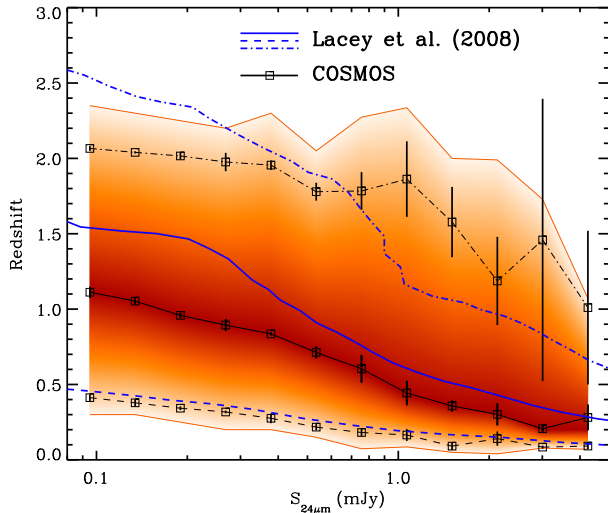
FIG. 10.— Comparison between our COSMOS flux/redshift distributions (thin lines and open symbols) and the predictions from the semi-analytical model of Lacey et al. (2008, thick curves, no symbol). For each bin of $24\,\mu$m flux the solid lines correspond to the median redshift while the dashed and dash-dotted lines represent the 10th and 90th percentiles of the associated distribution. Our error bars account for the uncertainties due to cosmic variance and Poisson noise as described in Sect. 4. The shaded region illustrates the parameter space populated by the MIPS-24 $\mu$m sources between the 5th and the 95th percentiles of their redshift distribution. This comparison reveals a systematic overestimate of the predicted median redshift at all $24\,\mu$m fluxes. [*See the electronic edition of the Journal for a color version of this figure.*]
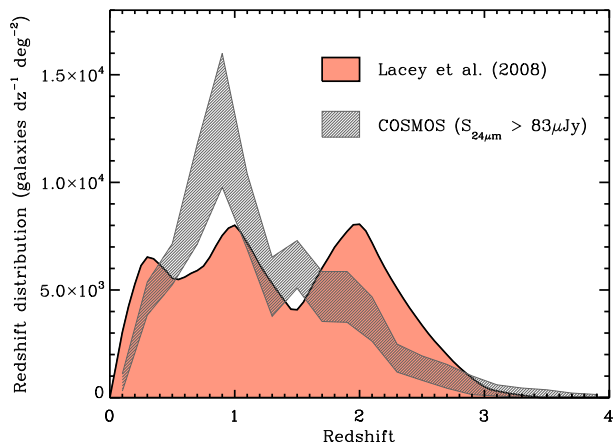


FIG. 11.— Total redshift distribution of the COSMOS $24\,\mu$m sources with $S_{24\mu m} > 83\,\mu$Jy (grey shaded region), compared with the model predictions of Lacey et al. (2008, solid line and filled histogram). The observed COSMOS distribution accounts for the uncertainties due to cosmic variance and Poisson noise as described in Sect. 4. Note the significant excess of sources predicted at $z \sim 2$ as well as the lack of $24\,\mu$m simulated galaxies at $z \sim 1$.



FIG. 12.— Redshift distributions of COSMOS $24\,\mu$m sources with $S_{24\mu m} > 83\,\mu$Jy decomposed into 3 bins of $K_s$–band *Vega* magnitude (grey shaded regions), compared with the model predictions of Lacey et al. (2008, solid lines and filled histograms). The observed distributions account for the uncertainties due to cosmic variance and Poisson noise as described in Sect. 4. Note the significant excess of sources predicted at $z \sim 2$ and mostly due to galaxies fainter than $K_s \sim 21.5$ mag, as well as the lack of $24\,\mu$m simulated sources with bright near-IR counterparts.

appearing in their model occurs mostly around $z \sim 2$. It originates from galaxies fainter than $K_s \sim 21.5$ mag (AB) while most of the $24\,\mu$m sources in our selection ($S_{24\mu m} > 83\,\mu$Jy) are typically brighter than this magnitude limit (see also, e.g., Papovich et al. 2007). On the other hand our comparison in the $r^+$–band reveals that these simulated sources are not particularly fainter than the typical $24\,\mu$m high redshift sources at optical wavelengths. In fact the redshift distribution of the $24\,\mu$m sources with faint optical fluxes seems to be rea-
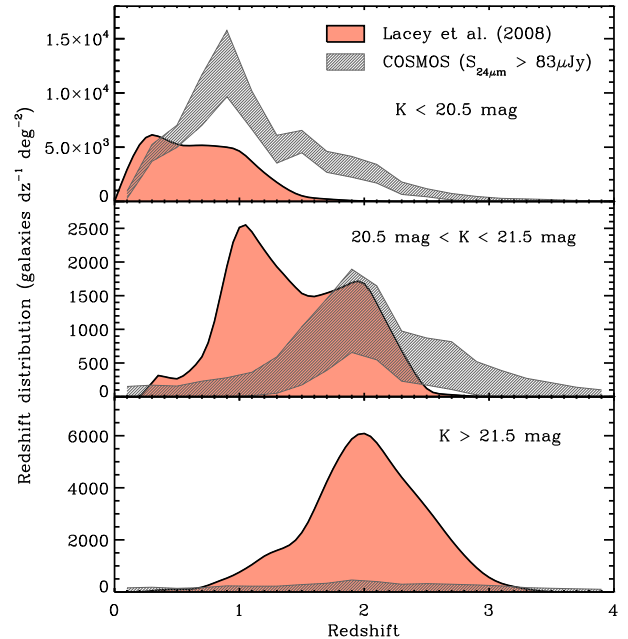
sonably well predicted (although the uncertainties due to the incompleteness of our redshift identification beyond $i^+_{AB} = 26.5$ mag prevents reaching definite conclusions). The excess of galaxies in the simulations originates from sources lying among the brightest optical counterparts associated with the $24\,\mu$m galaxy population at $z \sim 2$ (i.e., $r^+ \lesssim 25$ mag Vega) and it may thus be related to a too large number of blue galaxies predicted by the models.

Similarly we find that the lack of simulated galaxies noted by Lacey et al. (2008) at $z \sim 1$ is related to an underestimate of sources with relatively bright near-IR counterparts, while the predicted number of galaxies with fainter $K_s$–band luminosities ($K_s \gtrsim 20.5$ mag Vega) is clearly too large at this redshift. Given the slightly better agreement found at optical wavelengths, these results reveal again some discrepancies not only in the absolute optical/near-IR magnitudes of the predicted galaxies but also in their colors. We emphasize that this strong lack of $24\,\mu$m sources with bright near-IR luminosities (i.e., $K_s < 20.5$ mag Vega) is found at all redshifts from $z \sim 0.5$ to $z \sim 2.5$. Since the $K_s$–band emission of these distant sources should probe the rest-frame properties of their evolved stellar populations this may reflect a systematic underestimate of the density of massive galaxies with ongoing star formation in the distant Universe. Unfortunately though, we do not have access to the mock catalogs where the simulated $24\,\mu$m sources were extracted from. More detailed comparisons between the physical properties of the observed and the modeled galaxies will have to be performed to better understand the origin of
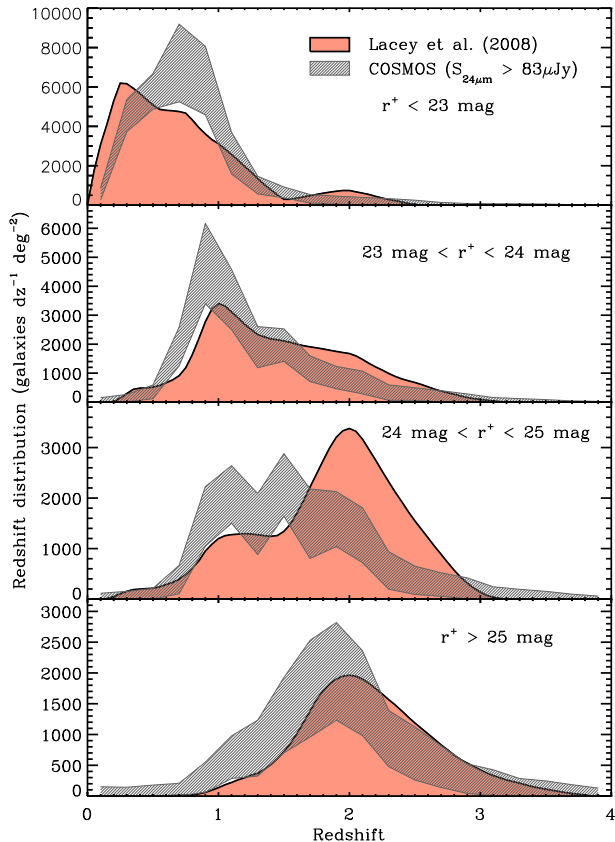
FIG. 13.— Redshift distributions of COSMOS $24\,\mu m$ sources with $S_{24\mu m} > 83\,\mu Jy$ decomposed into 4 different bins of $r^+$–band *Vega* magnitude (grey shaded regions), compared with the model predictions of Lacey et al. (2008, solid lines and filled histograms). The observed distributions account for the uncertainties due to cosmic variance and Poisson noise as described in Sect. 4. The predictions show a statistically better agreement than in the $K_s$– band (Fig. 12), although strong discrepancies can still be noted.

the discrepancies discussed above.

### 6.2. *Phenomenological models*

As shown above the understanding of the deep IR Universe with semi-analytical simulations still remains an important challenge for extragalactic astronomy. In the past few years, simpler descriptions accounting for the strong evolution of galaxy IR properties and based on "phenomenological" models have been proposed in the literature. Assuming a backward evolution of the local luminosity function and a library of galaxy spectral energy distributions, these models are usually constrained to reproduce a number of quantities like the Cosmic Infrared Background and/or galaxy IR properties such as the source number counts and redshift distributions. Although they can not be used to follow the history of the physical ingredients driving the evolution of galaxies and the change of their properties with time (e.g., gas accretion, stellar mass build-up, interactions, feedback, ...), they do not require a formalism as complex as the one needed in semi-analytical models. They can also be useful in planing the overall characteristics (e.g., source counts, redshift distribution, ...) of new IR or submillimeter surveys to be performed at yet-unexplored wavelengths.

All these models can vary from one another in the choice of their IR SED library, their decomposition of the overall galaxy population in different sub-groups (e.g., quiescent galaxies, starbursts, active nuclei, ...) or the parameterization characterizing how the luminosity function is allowed to vary with lookback time. In Figure 14 we present the comparison between our COSMOS $24\,\mu m$ source redshift distributions and the predictions from the phenomenological models of Le Borgne et al. (2009), Gruppioni et al. (2005, in prep.) and Lagache et al. (2004). Assuming the luminosity-dependent SED library from Chary & Elbaz (2001), Le Borgne et al. (2009) have used a non-parametric "count inversion" technique with no specific assumption on the evolution of the luminosity function to fit the most-recently updated results from *Spitzer* IR surveys. On the other hand the model presented by Gruppioni et al. (2005) did not make use of any *Spitzer* data but was constrained with $15\,\mu m$ observations carried out with the *Infrared Space Observatory*. It assumes four distinct populations of sources (quiescent galaxies, star-forming sources, type 1 and type 2 AGNs), each of them evolving independently from the others. Initially these populations were characterized by a single template SED (Gruppioni et al. 2005), but their scenario was recently updated to account for new procedures fitting individual galaxies with AGN and starburst SEDs simultaneously from the optical up to the mid-IR wavelengths (Gruppioni et al., in prep.). Finally, Lagache et al. (2004) assume a population of luminous starbursts characterized by luminosity-dependent SEDs as well as a population of quiescent cold galaxies evolving independently from the star-forming sources. Their model was updated from a previous version developed before the launch of *Spitzer* to account for the new constraints imposed at $24\,\mu m$ by the MIPS cosmological surveys.

The comparisons between these three models and our COSMOS data are illustrated for $24\,\mu m$ flux limits of 0.08, 0.15 and 0.3 mJy. The possible range of observed redshift distributions shown in the figure was calculated as described in Sect. 4 by taking into account the combined effect of flux and redshift uncertainties as well as the Poisson noise and the cosmic variance. We did not include any comparison below $z \sim 0.4$ as the small comoving volume sampled by our survey at these low redshifts would imply large statistical uncertainties. At $z \gtrsim 1$ and faint fluxes (e.g., $S_{24\mu m} \lesssim 0.15\,mJy$) we note that the model of Le Borgne et al. (2009) shows a rather good agreement with our observations, while the models from Gruppioni et al. (2005) and Lagache et al. (2004) show a significant overestimate of the number of $24\,\mu m$ sources around $z \sim 2$. As we discussed in Sect. 4 the bimodal distribution predicted by these two models is mainly produced by $k$-correction effects boosting the detectability of starburst sources when their $7.7\,\mu m$ aromatic feature is redshifted into the MIPS $24\,\mu m$ bandpass at $1.5 \lesssim z \lesssim 2.5$. The predicted bimodality is clearly not as prominent in the data. This disagreement could reflect either the presence of too strong features in the SEDs assumed by the models or a too rapid evolution of the source space density at the faintest fluxes typically probed by our survey. On the other hand, the break observed at $z \sim 1.3$ in the redshift distribution of the COSMOS galaxy population at bright fluxes seems
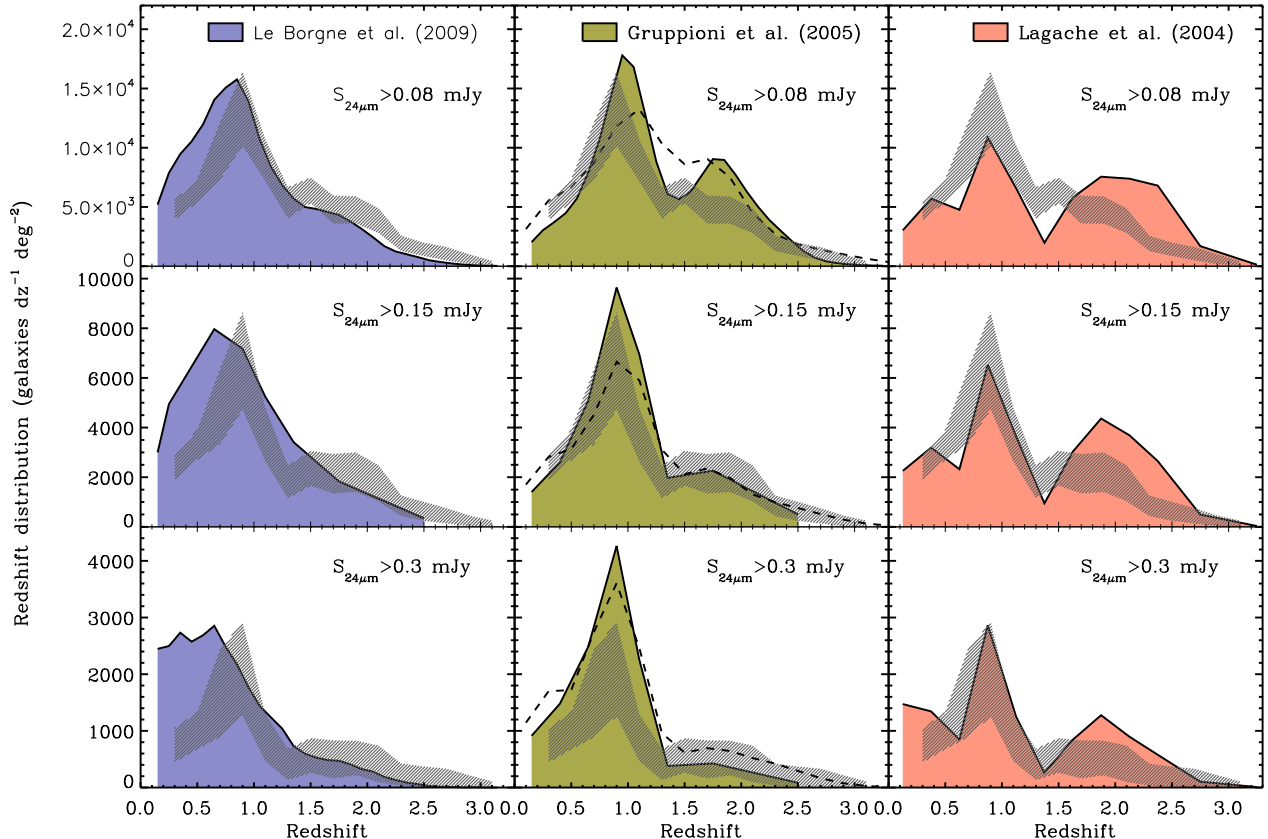
FIG. 14.— Comparison between our COSMOS redshift distributions (grey shaded regions) and the model predictions (solid lines and filled histograms) of Le Borgne et al. (2009, left panels), Gruppioni et al. (2005, middle panels) and Lagache et al. (2004, right panels), shown for 24 μm flux limits of 0.08, 0.15 and 0.3 mJy. The observed distributions account for the uncertainties due to cosmic variance and Poisson noise as described in Sect. 4. The dashed lines in the medium-column panels represent the predictions from a new version of the model developed by Gruppioni et al. (in prep., Gruppioni & Pozzi, private communication).

to be better reproduced by the model of Gruppioni et al. than in the predictions from Le Borgne et al. (where the break is barely apparent) or Lagache et al. (where the break is too prominent due to the strong excess of sources expected at $z \sim 2$). At $z \sim 1$ Gruppioni et al. (2005) predict however too many sources at $S_{24\mu m} \gtrsim 0.3$ mJy while the model of Le Borgne et al. may also overestimate the luminosity function at $0.4 \lesssim z \lesssim 0.8$.

## 7. DISCUSSION

Because of (i) the unprecedented accuracy of the photometric redshifts used in this work, (ii) our very high rate of redshift identifications obtained down to $S_{24\mu m} = 80\,\mu$Jy, and (iii) the large area covered by our survey, our analysis represents the most statistically significant characterization of the redshift distributions of the 24 μm source number counts achieved so far. We found that the distribution of the 24 μm selected galaxies is characterized by a prominent peak at $z \sim 1$ and a relatively large fraction of sources at $1 \lesssim z \lesssim 3$, which is globally consistent with the distributions of MIPS-24 μm sources previously determined with other surveys (Pérez-González et al. 2005; Caputi et al. 2006; Papovich et al. 2007; Desai et al. 2008). However, specific differences between our results and these other studies can be noticed. For instance, the redshift distribution obtained by Pérez-

González et al. (2005) shows a gradual and rapid decline from $z \sim 1$ up to $z \sim 3$, while we observe a break at $z \sim 1.3$ as well as a larger fraction of sources at $z \gtrsim 1$. Similarly, our distributions exhibit smoother variations than the redshift distribution determined by Caputi et al. (2006) in the field of the *Chandra Deep Field South* (CDFS). All these deviations from our results could originate either from less accurate photometric redshifts that were used in some of these other studies, or from the effect of cosmic variance over small fields of view like the CDFS.

The large number of 24 μm sources at $0.5 \lesssim z \lesssim 1.5$ and our analysis of the history of the 24 μm background light also shows that the CIB must originate predominantly from moderately-luminous galaxies at intermediate redshifts rather than highly obscured and luminous dusty sources at $z \gtrsim 2$. This result has already been inferred from previously-published studies (e.g., Elbaz et al. 2002; Dole et al. 2006) but our data provide for the first time a large enough statistics to explore with good accuracy the build-up of the mid-IR background as a function of cosmic time. The characterization of the far-IR properties of the 24 μm sources with the already-existing MIPS-70/160 μm and MAMBO-1.2 mm observations of COSMOS (Frayer et al., submitted; Bertoldi et al. 2007) or with the future coverage of this field with forthcoming facilities like *Herschel* will provide an even more detailed picture of the history of the EBL over the whole range

of IR wavelengths.

Yet, in spite of this globally coherent picture that has emerged from mid-IR surveys our comparison between the COSMOS $24\,\mu m$ data and the model predictions of Lacey et al. (2008) reveal that the evolution and the properties of luminous galaxies in the distant Universe are still far from being properly reproduced by the semi-analytical simulations of cosmic history. Although the rapid evolution of the IR luminosity function up to $z \sim 2$ is globally well predicted by the model of Lacey et al. (2008), discrepancies in the expected source density per bin of IR luminosity and in the optical/near-IR properties of $24\,\mu m$ sources are clearly apparent.

Interestingly we found that the number of $24\,\mu m$ sources with bright near-IR counterparts (i.e., $K_s \lesssim 20.5\,\text{mag}$ Vega) in the simulations is clearly underestimated at all redshifts beyond $z \sim 0.5$. It implies that the predicted source density of massive galaxies with strong on-going activity of star formation such as those recently discovered at high redshift with *Spitzer* (e.g., Daddi et al. 2005; Reddy et al. 2006; Papovich et al. 2006; Wuyts et al. 2008) is too low. Besides we note an overestimate of simulated sources with $20.5\,\text{mag} < K_s < 21.5\,\text{mag}$ (Vega) at $z \sim 1$, while their counterparts in the $r^+$–band seem to be more representative of the optical properties of $24\,\mu m$ sources at this redshift. In addition to the overall underestimate of the predicted source density at this redshift, we thus conclude that a large fraction of simulated galaxies at $z \sim 1$ are too blue with respect to the typical $24\,\mu m$ detected sources. This trend actually recalls the discrepancy that we also observed at $z \sim 2$ where the overestimate of predicted sources originates from blue galaxies with $K_s$–band luminosities much fainter than the bulk of $24\,\mu m$ sources found at this redshift.

The origin of this excess of blue galaxies with a $24\,\mu m$ detection above our sensitivity limit is not straight forward to determine. Assuming that the star formation rate (SFR) of individual sources is correctly predicted by the simulations, it may be related to an incorrect description of their spectral energy distributions. As we mentioned in Sect. 4 the broad aromatic features commonly observed at $7.7\,\mu m$, $11.3\,\mu m$ and $12.7\,\mu m$ in the spectra of starburst galaxies can enhance their detectability when these lines are redshifted into the MIPS-24 $\mu m$ bandpass. An overestimate of the strength of the $7.7\,\mu m$ feature could thus result in too many $24\,\mu m$ sources predicted at $z \sim 2$. Furthermore the $r^+$–band emission of galaxies at such high redshifts relates to their rest-frame UV properties, which are obviously very sensitive to dust extinction given our selection performed at mid-IR wavelengths. A wrong treatment of the obscuration affecting these $24\,\mu m$ sources would thus bias their predicted characteristics at optical wavelengths as well as the estimate of their reprocessed dust emission in the mid-infrared.

On the other hand, this excess could also originate from an overestimate of the galaxy star formation rate itself. In the simulations of Lacey et al. (2008) galaxies with on-going bursts of star formation account for $\sim 50\%$ and $\gtrsim 90\%$ the $24\,\mu m$ source population at $z \sim 1$ and $z \sim 2$ respectively (the other sources being classified as quiescent galaxies, see their Figure A4). Their mid-IR emission directly scales with their star-forming activity, which

could lead to a too large number of predicted sources if their SFR is statistically too high. Indeed, star formation processes critically depend on fundamental mechanisms and physical parameters that may still not be fully constrained in the simulations, like for instance the critical density above which stars can form depending on the galaxy internal dynamics and the various energy feedback (AGNs, supernovae, ...).

Finally, it is worth noting that the observed optical and near-IR colors may also depend on the Initial Mass Function (IMF) assumed in the simulations. In the model of Lacey et al. (2008) a normal neighborhood IMF leads to a too little evolution of the mid-IR luminosity function compared to the data, and it also underestimates the strong evolution observed in the faint submillimeter number counts (Baugh et al. 2005). A key ingredient characterizing their scenario is the use of a top-heavy IMF for the bursts of star formation triggered by galaxy mergers, which seems to better reproduce the evolution of the galaxy luminosity function observed in the mid-IR. Under this assumption though, the larger fraction of blue and massive stars produced in bursts should lead to bluer stellar populations and this could be one of the reasons explaining the excess of blue galaxies in their predictions. A much more detailed comparison between the intrinsic properties (mass, SFR, SEDs) of *individual* simulated sources and those characterizing the observed $24\,\mu m$ galaxy population will be necessary to identify the critical parameters that need to be better constrained for improving model predictions in the infrared.

Given the large number of ingredients to control, the determination of proper predictions of galaxy evolution at IR wavelengths with current semi-analytical models remains obviously a challenging task. Reproducing the evolution of the IR luminosity function requires not only an accurate description of the evolution of the bolometric luminosity function for star-forming galaxies but also an accurate treatment of dust extinction as a function of galaxy properties and a reliable representation of galaxy SEDs in the infrared. Furthermore, dust-obscured star-forming galaxies are not the only contributers to the number counts at IR wavelengths. Quasars and dusty AGNs should also be taken into account, especially at the bright end of the luminosity function where their contribution is far from being negligible (e.g., Brand et al. 2006). Given the coeval growth of bulges and super-massive black holes (e.g., Page et al. 2001) "composite" sources experiencing both nuclear and star-forming activity may actually represent a large fraction of the mid-IR selected galaxy population at high redshift. This large variety of physical properties characterizing IR-luminous galaxies added to the complexity of their spectral signatures in the mid-IR can thus make the predictions from semi-analytical simulations particularly difficult at IR wavelengths.

This contribution of nuclear accretion to cosmic history has not been implemented in the model of Lacey et al. (2008). Therefore the feedback action of AGNs, which has been recently discussed in the framework of other semi-analytical models as an efficient process to regulate the star-forming activity in galaxies, is not taken into account in their simulations. Instead, the decrease of gas cooling for the formation of massive spheroids is controlled in their model by the action of superwinds driven

by supernova explosions. These winds produce a feedback effect qualitatively similar to that of AGNs, but the underlying physical mechanisms are somehow different and they result in different predictions for the evolution of the galaxy luminosity function with redshift (Lacey et al. 2008). Infrared simulations of distant sources accounting for the role of AGN feedback were actually presented by Silva et al. (2005) using the model of Granato et al. (2004). However their scenario did not directly include the merging of galaxies and dark matter haloes, and contrary to our results their $24\,\mu m$ source redshift distribution at $S_{24\mu m} > 0.2\,\mathrm{mJy}$ was predicted to peak at $z \sim 2$. Given the current $\Lambda$CDM paradigm as well as the role that nuclear accretion played in the evolution of dusty high redshift galaxies, one possible approach to progress in our understanding of the deep IR Universe with semi-analytical models would be therefore to explore the impact of scenarios including both the hierarchical assembly of dark matter haloes and the contribution of AGNs.

## 8. SUMMARY

We performed our very first analysis of the deep $24\,\mu m$ observations carried out with the *Spitzer Space Telescope* over the $2\,\mathrm{deg}^2$ of the COSMOS field. We detected almost $\sim 30\,000$ sources down to a $24\,\mu m$ flux of $80\,\mu\mathrm{Jy}$. Using the multi-wavelength ancillary data available in COSMOS we identified the optical/near-IR counterparts and the photometric redshifts for $\sim 95\%$ of these $24\,\mu m$ detections. The main results that we derived can be summarized as follows:

1. The redshift distribution of the $24\,\mu m$–selected galaxies shows a prominent peak at $z \sim 1$ but more than $\sim 50\%$ of the sample is located at $1 \lesssim z \lesssim 3$. Below $z \sim 1$ almost all $24\,\mu m$ sources are brighter than $24\,\mathrm{mag}$ (AB) in the $i^+$–band, while a non-negligible of the MIPS sources at higher redshifts are associated with very faint optical counterparts (i.e., $24\,\mathrm{mag} \lesssim i^+ \lesssim 26.5\,\mathrm{mag}$).

2. Below a fixed optical magnitude limit the fraction of $i^+$–band sources with $24\,\mu m$ detection strongly increases up to $z \sim 2$. This reflects the strong evolution that star-forming galaxies have undergone with lookback time. However this rising trend shows a clear break at $z \sim 1.3$, which seems to be more pronounced when higher $24\,\mu m$ flux selections are considered (e.g., $S_{24\mu m} \gtrsim 0.3\,\mathrm{mJy}$). This feature is also visible in the redshift distributions of $24\,\mu m$ sources. It probably originates from $k$-correction effects implied by the presence of the strong aromatic features and/or the Silicate absorption commonly observed in the spectra of luminous dusty galaxies.

3. Using extrapolations of the number counts at faint fluxes we resolved the build-up of the mid-infrared background across cosmic ages. We find that $\sim 50\%$ and $\sim 80\%$ of the $24\,\mu m$ background intensity originate from galaxies at $z \lesssim 1$ and $z \lesssim 2$ respectively, with a contribution of faint sources reaching $\sim 20 \pm 10\%$ below our detection limit. As already suggested by other previously-published studies we thus infer that the Cosmic Infrared Background is mostly produced by moderately-luminous dusty galaxies at $0.5 \lesssim z \lesssim 1.5$ rather than very luminous and obscured sources at $z \gtrsim 2$.

4. The comparison between our results and semi-analytical predictions reveal substantial discrepancies in the simulated redshift distributions as well as in the $R - K$ colors of the $24\,\mu m$ source counterparts. In particular we found a strong excess of blue sources predicted at $z \sim 2$ and the $K$–band fluxes of simulated galaxies appear to be systematically too low at $z \gtrsim 0.5$. This could reflect an underestimate of the density of high redshift massive sources with strong on-going star formation possibly related to fundamental physical parameters and/or processes that are still not fully constrained in the simulations of galaxy formation. It could also be due to an inaccurate treatement of dust extinction in the models, which would imply discrepancies in the predictions of the galaxy SEDs at rest-frame UV, optical and mid-IR wavelengths.

5. Comparisons with some of the most recent backward evolution scenarios reproduce reasonably well the flux/redshift distribution of $24\,\mu m$ sources up to $z \sim 3$. Nonetheless none of them is able to accurately match our results at all redshifts over the full range of $24\,\mu m$ fluxes probed by our survey.

## REFERENCES

Alonso-Herrero, A., Pérez-González, P. G., Alexander, D. M., et al. 2006, ApJ, 640, 167

Armus, L., Charmandaris, V., Bernard-Salas, J., et al. 2007, ApJ, 656, 148

Aussel, H., Cesarsky, C. J., Elbaz, D., & Starck, J. L. 1999, A&A, 342, 313

Bai, L., Marcillac, D., Rieke, G. H., et al. 2007, ApJ, 664, 181

Barger, A. J., Cowie, L. L., Sanders, D. B., et al. 1998, Nature, 394, 248

Baugh, C. M., Lacey, C. G., Frenk, C. S., et al. 2005, MNRAS, 356, 1191

Bavouzet, N., Dole, H., Le Floc'h, E., et al. 2008, A&A, 479, 83

Bertin, E. & Arnouts, S. 1996, A&AS, 117, 393

Bertoldi, F., Carilli, C., Aravena, M., et al. 2007, ApJS, 172, 132

Blain, A. W., Chapman, S. C., Smail, I., & Ivison, R. 2004, ApJ, 611, 52

Blain, A. W., Smail, I., Ivison, R. J., & Kneib, J.-P. 1999, MNRAS, 302, 632

Blain, A. W., Smail, I., Ivison, R. J., Kneib, J.-P., & Frayer, D. T. 2002, Phys. Rep., 369, 111

Blaizot, J., Szapudi, I., Colombi, S., et al. 2006, MNRAS, 369, 1009

Borys, C., Blain, A. W., Dey, A., et al. 2006, ApJ, 636, 134

Bower, R. G., Benson, A. J., Malbon, R., et al. 2006, MNRAS, 370, 645

Brand, K., Dey, A., Weedman, D., et al. 2006, ApJ, 644, 143

Brandl, B. R., Bernard-Salas, J., Spoon, H. W. W., et al. 2006, ApJ, 653, 1129

Bridge, C. R., Appleton, P. N., Conselice, C. J., et al. 2007, ApJ, 659, 931

Brusa, M., Zamorani, G., Comastri, A., et al. 2007, ApJS, 172, 353

Buat, V., Boissier, S., Burgarella, D., et al. 2008, A&A, 483, 107

Capak, P., Aussel, H., Ajiki, M., et al. 2007, ApJS, 172, 99

Caputi, K. I., Dole, H., Lagache, G., et al. 2006, ApJ, 637, 727

Cattaneo, A., Dekel, A., Devriendt, J., Guiderdoni, B., & Blaizot, J. 2006, MNRAS, 370, 1651

Chary, R., Casertano, S., Dickinson, M. E., et al. 2004, ApJS, 154, 80

Chary, R. & Elbaz, D. 2001, ApJ, 556, 562

Cole, S., Lacey, C. G., Baugh, C. M., & Frenk, C. S. 2000, MNRAS, 319, 168

Croton, D. J., Springel, V., White, S. D. M., et al. 2006, MNRAS, 365, 11

da Cunha, E., Charlot, S., & Elbaz, D. 2008, MNRAS, 388, 1595

Daddi, E., Dickinson, M., Chary, R., et al. 2005, ApJ, 631, L13

Dale, D. A., Smith, J. D. T., Armus, L., et al. 2006, ApJ, 646, 161

de Grijp, M. H. K., Miley, G. K., Lub, J., & de Jong, T. 1985, Nature, 314, 240

Desai, V., Soifer, B. T., Dey, A., et al. 2008, ApJ, 679, 1204

Dey, A., Soifer, B. T., Desai, V., et al. 2008, ApJ, 677, 943

Dole, H., Lagache, G., Puget, J.-L., et al. 2006, A&A, 451, 417

Dole, H., Le Floc'h, E., Pérez-González, P. G., et al. 2004, ApJS, 154, 87

Dopita, M. A., Groves, B. A., Fischera, J., et al. 2005, ApJ, 619, 755

Downes, D., Neri, R., Greve, A., et al. 1999, A&A, 347, 809

Elbaz, D., Cesarsky, C. J., Chanial, P., et al. 2002, A&A, 384, 848

Elbaz, D., Cesarsky, C. J., Fadda, D., et al. 1999, A&A, 351, L37

Elbaz, D., Daddi, E., Le Borgne, D., et al. 2007, A&A, 468, 33

Engelbracht, C. W., Blaylock, M., Su, K. Y. L., et al. 2007, PASP, 119, 994

Fiore, F., Grazian, A., Santini, P., et al. 2008, ApJ, 672, 94

Franceschini, A., Aussel, H., Cesarsky, C. J., Elbaz, D., & Fadda, D. 2001, A&A, 378, 1

Frayer, D. T., Fadda, D., Yan, L., et al. 2006, AJ, 131, 250

Genzel, R., Lutz, D., Sturm, E., et al. 1998, ApJ, 498, 579

Gordon, K. D., Clayton, G. C., Witt, A. N., & Misselt, K. A. 2000, ApJ, 533, 236

Gorlova, N., Rieke, G. H., Muzerolle, J., et al. 2006, ApJ, 649, 1028

Granato, G. L., De Zotti, G., Silva, L., Bressan, A., & Danese, L. 2004, ApJ, 600, 580

Gruppioni, C., Pozzi, F., Lari, C., Oliver, S., & Rodighiero, G. 2005, ApJ, 618, L9

Hasinger, G., Cappelluti, N., Brunner, H., et al. 2007, ApJS, 172, 29

Houck, J. R., Roellig, T. L., van Cleve, J., et al. 2004, ApJS, 154, 18

Houck, J. R., Soifer, B. T., Weedman, D., et al. 2005, ApJ, 622, L105

Huang, J.-S., Rigopoulou, D., Willner, S. P., et al. 2005, ApJ, 634, 137

Hughes, D. H., Serjeant, S., Dunlop, J., et al. 1998, Nature, 394, 241

Ilbert, O., Capak, P., Salvato, M., et al. 2009, ApJ, 690, 1236

Jarrett, T. H., Chester, T., Cutri, R., et al. 2000, AJ, 119, 2498

Koekemoer, A. M., Aussel, H., Calzetti, D., et al. 2007, ApJS, 172, 196

Lacey, C. G., Baugh, C. M., Frenk, C. S., et al. 2008, MNRAS, 385, 1155

Lagache, G., Dole, H., Puget, J.-L., et al. 2004, ApJS, 154, 112

Laurent, O., Mirabel, I. F., Charmandaris, V., et al. 2000, A&A, 359, 887

Le Borgne, D., Elbaz, D., Ocvirk, P., & Pichon, C., 2009, A&A, in press (astro-ph/0901.3783)

Le Floc'h, E., Willmer, C. N. A., Noeske, K., et al. 2007, ApJ, 660, L65

Lilly, S. J., Le Fèvre, O., Renzini, A., et al. 2007, ApJS, 172, 70

Lutz, D., Sturm, E., Tacconi, L. J., et al. 2008, ApJ, 684, 853

Makovoz, D. & Khan, I. 2005, in Astronomical Society of the Pacific Conference Series, Vol. 347, Astronomical Data Analysis Software and Systems XIV, ed. P. Shopbell, M. Britton, & R. Ebert, 81

Marcillac, D., Rieke, G. H., Papovich, C., et al. 2008, ApJ, 675, 1156

Marleau, F. R., Fadda, D., Storrie-Lombardi, L. J., et al. 2004, ApJS, 154, 66

Marshall, J. A., Herter, T. L., Armus, L., et al. 2007, ApJ, 670, 129

Mazzarella, J. M., Bothun, G. D., & Boroson, T. A. 1991, AJ, 101, 2034

Menéndez-Delmestre, K., Blain, A. W., Alexander, D. M., et al. 2007, ApJ, 655, L65

Nenkova, M., Ivezić, Ž., & Elitzur, M. 2002, ApJ, 570, L9

Noeske, K. G., Faber, S. M., Weiner, B. J., et al. 2007, ApJ, 660, L47

Page, M. J., Stevens, J. A., Mittaz, J. P. D., & Carrera, F. J. 2001, Science, 294, 2516

Papovich, C., Dole, H., Egami, E., et al. 2004, ApJS, 154, 70

Papovich, C., Moustakas, L. A., Dickinson, M., et al. 2006, ApJ, 640, 92

Papovich, C., Rudnick, G., Le Floc'h, E., et al. 2007, ApJ, 668, 45

Pérez-González, P. G., Rieke, G. H., Egami, E., et al. 2005, ApJ, 630, 82

Polletta, M. d. C., Wilkes, B. J., Siana, B., et al. 2006, ApJ, 642, 673

Pope, A., Chary, R.-R., Alexander, D. M., et al. 2008, ApJ, 675, 1171

Pope, A., Scott, D., Dickinson, M., et al. 2006, MNRAS, 370, 1185

Reddy, N. A., Steidel, C. C., Fadda, D., et al. 2006, ApJ, 644, 792

Reddy, N. A., Steidel, C. C., Pettini, M., et al. 2008, ApJS, 175, 48

Rieke, G. H., Blaylock, M., Decin, L., et al. 2008, AJ, 135, 2245

Rieke, G. H., Young, E. T., Engelbracht, C. W., et al. 2004, ApJS, 154, 25

Rodighiero, G., Lari, C., Pozzi, F., et al. 2006, MNRAS, 371, 1891

Sajina, A., Yan, L., Armus, L., et al. 2007, ApJ, 664, 713

Salvato, M., Hasinger, G., Ilbert, O., et al. 2009, ApJ, 690, 1250

Sanders, D. B., Salvato, M., Aussel, H., et al. 2007, ApJS, 172, 86

Schinnerer, E., Smolčić, V., Carilli, C. L., et al. 2007, ApJS, 172, 46

Scoville, N., Abraham, R. G., Aussel, H., et al. 2007a, ApJS, 172, 38

Scoville, N., Aussel, H., Brusa, M., et al. 2007b, ApJS, 172, 1

Shupe, D. L., Rowan-Robinson, M., Lonsdale, C. J., et al. 2008, AJ, 135, 1050

Siebenmorgen, R. & Krügel, E. 2007, A&A, 461, 445

Silva, L., De Zotti, G., Granato, G. L., Maiolino, R., & Danese, L. 2005, MNRAS, 357, 1295

Silva, L., Granato, G. L., Bressan, A., & Danese, L. 1998, ApJ, 509, 103

Smail, I., Ivison, R. J., & Blain, A. W. 1997, ApJ, 490, L5

Smith, J. D. T., Draine, B. T., Dale, D. A., et al. 2007, ApJ, 656, 770

Somerville, R. S., Hopkins, P. F., Cox, T. J., Robertson, B. E., & Hernquist, L. 2008, MNRAS, 391, 481

Spergel, D. N., Verde, L., Peiris, H. V., et al. 2003, ApJS, 148, 175

Spinoglio, L., Malkan, M. A., Rush, B., Carrasco, L., & Recillas-Cruz, E. 1995, ApJ, 453, 616

Spoon, H. W. W., Marshall, J. A., Houck, J. R., et al. 2007, ApJ, 654, L49

Springel, V., Di Matteo, T., & Hernquist, L. 2005, MNRAS, 361, 776

Stetson, P. B. 1987, PASP, 99, 191

Symeonidis, M., Willner, S. P., Rigopoulou, D., et al. 2008, MNRAS, 385, 1015

Taniguchi, Y., Scoville, N., Murayama, T., et al. 2007, ApJS, 172, 9

Webb, T. M. A., van Dokkum, P., Egami, E., et al. 2006, ApJ, 636, L17

Weedman, D. W., Hao, L., Higdon, S. J. U., et al. 2005, ApJ, 633, 706

Werner, M. W., Roellig, T. L., Low, F. J., et al. 2004, ApJS, 154, 1

Wu, Y., Charmandaris, V., Hao, L., et al. 2006, ApJ, 639, 157

Wuyts, S., Labbé, I., Schreiber, N. M. F., et al. 2008, ApJ, 682, 985

Yan, L., Chary, R., Armus, L., et al. 2005, ApJ, 628, 604